

**Obstruction to ergodicity in nonlinear Schrödinger equations with resonant potentials**Anxo Biasi <sup>1</sup>, Oleg Evnin <sup>2,3</sup>, and Boris A. Malomed <sup>4,5</sup><sup>1</sup>*Laboratoire de Physique de l'Ecole Normale Supérieure ENS Université PSL, CNRS, Sorbonne Université, Université de Paris, F-75005 Paris, France*<sup>2</sup>*Department of Physics, Faculty of Science, Chulalongkorn University, Bangkok 10330, Thailand*<sup>3</sup>*Theoretische Natuurkunde, Vrije Universiteit Brussel and International Solvay Institutes, Brussels 1050, Belgium*<sup>4</sup>*Department of Physical Electronics, School of Electrical Engineering, Tel Aviv University, Tel Aviv 69978, Israel*<sup>5</sup>*Instituto de Alta Investigación, Universidad de Tarapacá, Casilla 7D, Arica, Chile*

(Received 29 April 2023; accepted 11 August 2023; published 8 September 2023)

We identify a class of trapping potentials in cubic nonlinear Schrödinger equations (NLSEs) that make them nonintegrable, but prevent the emergence of power spectra associated with ergodicity. The potentials are characterized by equidistant energy spectra (e.g., the harmonic-oscillator trap), which give rise to a large number of resonances enhancing the nonlinearity. In a broad range of dynamical solutions, spanning the regimes in which the nonlinearity may be either weak or strong in comparison with the linear part of the NLSE, the power spectra are shaped as narrow (quasidiscrete), evenly spaced spikes, unlike generic truly continuous (ergodic) spectra. We develop an analytical explanation for the emergence of these spectral features in the case of weak nonlinearity. In the strongly nonlinear regime, the presence of such structures is tracked numerically by performing simulations with random initial conditions. Some potentials that prevent ergodicity in this manner are of direct relevance to Bose-Einstein condensates: they naturally appear in 1D, 2D, and 3D Gross-Pitaevskii equations (GPEs), the quintic version of these equations, and a two-component GPE system.

DOI: [10.1103/PhysRevE.108.034204](https://doi.org/10.1103/PhysRevE.108.034204)**I. INTRODUCTION**

The clash between integrability and ergodic behavior is a well-known basic phenomenon in the dynamics of nonlinear systems [1,2]. While the evolution of generic systems with many degrees of freedom typically exhibits thermalization, chaotization, and stochasticity, dynamics of integrable systems are tightly constrained by a large (or infinite) number of conservation laws. A conflict between these scenarios arises when the system is “close” to integrability [1]. In that case, a natural question is to what extent the dynamics displays ergodic features. Such questions were suggested, in particular, two decades ago by experiments with nearly 1D cold atomic gases [3,4] because the underlying basic model may be the integrable Lieb-Liniger one [5], but integrability-breaking effects cannot be completely eliminated from the real-world setup [6]. The problem of the competition between the integrability and ergodicity motivated studies of deviations from the standard framework of nonequilibrium dynamics [7], bringing along intriguing ideas such as generalized hydrodynamics [8–14], prethermalization [15–18], generalized Gibbs ensembles [19–21], etc.

A common approach to analytical and numerical studies of these problems relies on perturbing an integrable equation by extra terms—typically, this is an external trap added to the nonlinear Schrödinger equation (NLSE) [11,22]. Then, one explores consequences of the integrability breaking in the perturbed model [11,12,18,22–24]. One may, however, wonder whether a *mechanism other than integrability* exists to produce essential deviations from ergodic signatures of nonintegrable dynamics. This question underlies the present work, leading to

a class of NLSEs including *highly resonant potentials* (HRP), namely, ones that, for the linear Schrödinger equation, yield equidistant spectra of energy eigenvalues  $E_n$ :

$$E_n = an + b, \quad (1)$$

with integer  $n$  and real constants  $a$  and  $b$ . A commonly known example is the harmonic-oscillator (HO) potential, whose equidistant spectrum is a consequence of the hidden symmetry of the respective quantum Hamiltonian [25]. Similarly, the equidistant structure of spectra of other potentials is related to their symmetries [26].

The term *highly resonant* reflects extreme abundance of resonances in these systems. Indeed, the equidistant positioning of eigenvalues in Eq. (1) ensures that the four-wave constraint,  $E_n + E_m - E_l - E_j = 0$  with integers  $n, m, l, j$ , which is the resonance condition for the cubic nonlinearity, reduces to a simple relation between the integer numbers,  $n + m - l - j = 0$ . It implies an infinite number of resonances for any mode ( $n = l + j - m$ ). It is shown below that the special structure of energy eigenvalues (1) has a strong impact on the dynamics, producing a regime of nonergodic evolution, in contrast with the generic (nonequidistant) energy spectra. This phenomenon is demonstrated, in particular, by the power spectra for the cubic NLSE with the HO potential displayed in Fig. 1. In the case of generic trapping potentials, the system indiscriminately excites a large range of frequencies, leading to ergodic (continuous and unstructured) power spectra [27], as shown in Figs. 1(b) and 1(c), which correspond, respectively, to the infinitely deep square well and an anharmonic potential. By contrast, HRPs, in a parameter range spanning regimes in which the cubic nonlinearity may be weak or strong, in

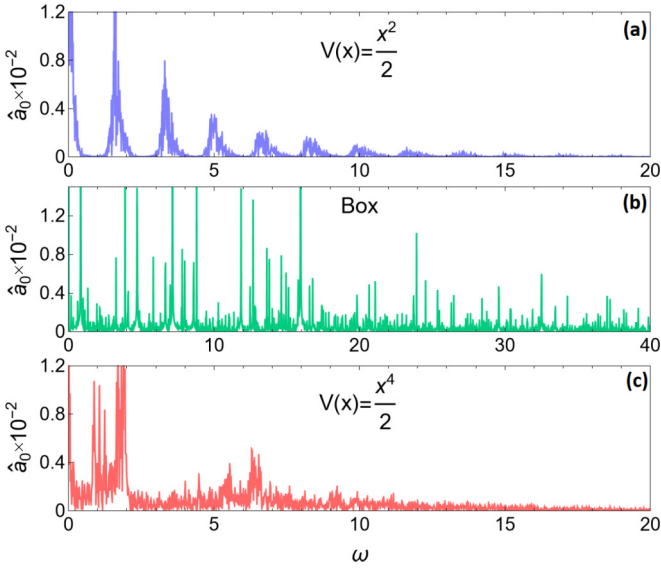


FIG. 1. The contrast between power spectra of the first-mode amplitude  $\hat{a}_0$ , defined according to Eq. (11), as produced by the numerical solution of the one-dimensional NLSE with the HO potential (a), infinitely deep square potential well (b), and quartic potential (c), initialized by the input with a random phase and amplitude. Amplitudes of higher modes produce similar plots.

comparison to the linear part of the NLSE, give rise to unusually depopulated power spectra, in which the excited frequencies reside in a “*comblike*” arrangement of spikes, as shown in Fig. 1(a). The comblike spectra induced by HRPVs reveal an *obstruction to ergodicity*, being drastically different from the continuously distributed spectra created by the generic traps. This conclusion is upheld by the similarity of the comblike power spectra in HRPVs to the discrete power spectra which are a characteristic feature of the integrable dynamics. The truly discrete spectra are associated with periodic and quasiperiodic trajectories that the integrable dynamics track on the surface of invariant tori in the phase space (with a very small share of the invariant tori being destroyed by integrability-breaking perturbations, according to the KAM theorem [28]).

Our motivation to search for alternatives to exact integrability in explaining nonergodic behavior came from specific results for the 1D Gross-Pitaevskii equation (GPE) [29,30], which is a well-established model for the dynamics of atomic Bose-Einstein condensates, based on the NLSE for the mean-field wave function of the condensate [31–33]. It is commonly known that the NLSE is integrable in the free 1D space [34,35], thus providing a good starting point for the study of the integrability-ergodicity clash. The dynamical behavior in the presence of an external trap, which breaks integrability [36], has been addressed for nonequilibrium configurations [27,37–43], coherent states in time-dependent traps [44,45], and propagation of a small number of solitons [46–55] (see also Refs. [56–66] for related models). Numerical works [46–49] suggested remarkable contrast between the GPE with the HO potential, and the equation including either anharmonic potentials or the infinitely deep potential box, which is represented by zero boundary conditions at the box edges.

In particular, a single dark soliton trapped in the box potential displays a continuous power spectrum, in consonance with ergodicity and indicating the emission of radiation [49]. However, the evolution of the dark soliton governed by the GPE with the HO potential gives rise to a quasidiscrete power spectrum, reminiscent of discrete spectra associated with the quasiperiodic dynamics of integrable systems [49]. The nonergodic behavior of the 1D GPE with the HO potential, as opposed to the apparent ergodicity maintained by other potentials, is not restricted to the soliton motion, but also happens for more generic initial conditions, such as random waves. As shown in Fig. 1, the evolution initialized by these configurations in the case of the HO potential displays comblike power spectra, while ergodic ones (truly continuous and unstructured) are seen in case of the box and quartic potentials. The specific shape of the power spectra supported by the HO potential suggests the presence of an underlying mechanism constraining the dynamics to a nonergodic form. It was referred to as “quasi-integrability” in Ref. [49], because, as said above, discrete spectra are a hallmark of integrable systems.

NLSEs with the HO potential display peculiar behavior which is not restricted to 1D. In particular, in 2D there are analytical solutions describing periodically modulated motion of a single-vortex [67] and multi-vortex configurations [68–70], as well as dark rings [69], as well as analytical and numerical manifestations of Fermi-Pasta-Ulam recurrences [70]. In Ref. [71], the rich structure exhibited by weakly nonlinear dynamics of the 2D GPE with the HO potential was extended to a large family of related systems with similar behaviors, and in Ref. [72], it was connected to the presence of breathing modes [73,74]. Another setup where the HO potential has shown quasiperiodic motions is the 1D quintic NLSE [75].

The connection between the 2D GPE with the HO potential and other systems with equidistant linear spectra subject to condition (1), which were considered in Refs. [71,72,75], is an incentive to find out whether the quasi-integrability of the 1D GPE with the HO potential, established in Ref. [49], is an exceptional feature, or, on the contrary, it is shared by a large class of NLSEs. To this end, we here examine the role played by the potential and conclude that comblike power spectra similar to the one plotted in Fig. 1(a) are displayed by NLSEs with HRPVs, whose linear spectra of energy eigenvalues take the form of Eq. (1). However, NLSEs with potentials that do not obey definition (1) do not display comblike spectra either, even if the spectra admit resonances between some modes.

Our results suggest three essential implications. First, NLSEs including HRPVs constitute a broad class of models ranging from some of the most common and physically relevant ones, such as the GPE with the HO potential in any number of spatial dimensions, to more sophisticated potentials [e.g., the one accounting for the “superselection,” see Eq. (30)] and nonlinear terms. The availability of 2D and 3D models of this type is particularly interesting for the experiment because they overcome fundamental limitations inherent to studies of weakly broken integrable dynamics. First, the perturbation theory applies, in the traditional form, solely to 1D models [36]. The second lifted limitation, which is related to the first one, is that our models are not necessarily produced by deformations of integrable equations. An example is the 1D quintic NLSE with the HO potential, which features

nonergodic power spectra without proximity to an exactly integrable equation (see details below). Finally, it is relevant to stress that our results offer an example of how a linear property, viz., the equidistant linear energy spectrum (1), may impose a fundamental constraint on the full nonlinear dynamics, preventing the onset of ergodicity. For our exposition of the results we mostly refer to two models, the 1D GPEs with the HO and box potentials, which represent the HRP and non-HRPs, respectively. Then, we explain how similar results are produced by other potentials.

The rest of the paper is organized as follows. First, we introduce the setup and make a direct comparison between the dynamics under the action of the HO and box potential in Sec. II. Then, in Sec. III we develop an analytical approximation for the power spectrum in the case of weak nonlinearity, which makes it possible to explain differences between the respective power spectra. Afterward, in Sec. IV we show numerically how the comblike power spectrum depends on the magnitude and sign (defocusing/focusing) of the nonlinear terms. This is followed in Sec. V by the presentation of comblike power spectra produced by *eleven* other HRP models, which provide a robust confirmation of the genericity of our results. The paper is concluded, in Sec. VI, by a discussion of prospects and implications of our findings. Some technical aspects of numerical methods employed in this work are presented in the Appendices.

## II. ONE-DIMENSIONAL GROSS-PITAEVSKII EQUATIONS WITH THE HARMONIC POTENTIAL AND BOX POTENTIALS

Throughout this paper, we use the 1D GPE with the cubic nonlinearity as the main setup to illustrate the methods and results. In Sec. V, we describe several other models, related to the ones addressed here. The scaled form of the GPE, with time  $t$  and coordinate  $x$ , is

$$i\partial_t\psi = -\frac{1}{2}\partial_x^2\psi + V(x)\psi + g|\psi|^2\psi, \quad (2)$$

where  $V(x)$  is the potential, and  $g$  the nonlinearity coefficient, with  $g > 0$  and  $g < 0$  representing the repulsive and attractive self-interactions, respectively. This equation conserves the norm

$$M = \int_{-\infty}^{+\infty} |\psi|^2 dx, \quad (3)$$

and energy (Hamiltonian)

$$H = \int_{-\infty}^{+\infty} \left( \frac{1}{2} |\nabla\psi|^2 + V(x)|\psi|^2 + \frac{g}{2} |\psi|^4 \right) dx, \quad (4)$$

which includes the quadratic and quartic parts, associated with the linear and nonlinear terms in Eq. (2), respectively:

$$H_2 = \int_{-\infty}^{+\infty} \left( \frac{1}{2} |\nabla\psi|^2 + V(x)|\psi|^2 \right) dx, \quad (5)$$

$$H_4 = \frac{g}{2} \int_{-\infty}^{+\infty} |\psi|^4 dx. \quad (6)$$

We fix the normalization by setting  $M = 1$  in Eq. (3). The equation will be studied in the full range from the weakly nonlinear regime ( $|g| \ll 1$ ) to the strongly nonlinear one ( $|g| \gg 1$ ). As said above, the latter case represents the situation in

which the cubic term is large in comparison with the linear ones, but higher-order nonlinear terms are still negligible. Normally, such terms do not appear in the GPE, except for the specially designed configuration, in which the cubic cross-attraction between two components of a binary BEC is nearly compensated by the self-repulsion in each component, making it necessary to consider the quartic self-repulsion, that represents effects of quantum fluctuations around the respective mean-field states, thus giving rise to the *quantum droplets* [76,77].

The HO and box potentials are our representative examples, chosen to illustrate the differences between HRP and non-HRP cases, respectively:

$$\text{HO} : V(x) = \frac{1}{2}x^2, \quad \text{box} : \begin{cases} 0, & \text{for } x \in (0, L), \\ \infty, & \text{elsewhere,} \end{cases} \quad (7)$$

where the coefficient of the HO potential is fixed by scaling to be 1,  $L$  is the size of the box, and the Dirichlet boundary conditions  $\psi(t, 0) = \psi(t, L) = 0$  are implied in the latter case.

The linearized version of Eq. (2) ( $g = 0$ ) gives rise to the commonly known eigenvalues  $E_n$  and eigenfunctions  $f_n(x)$ :

$$\text{HO} : E_n = n + \frac{1}{2}, \quad f_n(x) = \frac{H_n(x)}{\pi^{1/4} \sqrt{2^n n!}} e^{-x^2/2}, \quad (8)$$

$$\text{box} : E_n = \frac{\pi^2(n+1)^2}{2L^2}, \quad f_n(x) = \sqrt{\frac{2}{L}} \sin \frac{\pi(n+1)x}{L}, \quad (9)$$

where  $n \geq 0$  is the number of the bound state, and  $H_n(x)$  are Hermite polynomials. We fix  $L = \pi/\sqrt{2}$  for the box, to facilitate the comparison of power spectra produced by the two models. The fact that the HO potential belongs to the class of HRP is determined by its commonly known equidistant energy spectrum (8), while the quadratic spectrum (9) clearly indicates that the box potential belongs to the non-HRP class. It admits some resonances among its modes, but much fewer than enabled by the equidistant spectrum.

In both cases, the sets of eigenstates  $f_n(x)$  are used to rewrite the solution to Eq. (2) in terms of complex mode amplitudes  $\alpha_n(t)$ , defined so that

$$\psi(t, x) = \sum_{n=0}^{\infty} \alpha_n(t) f_n(x) e^{-iE_n t}. \quad (10)$$

The power spectrum of each amplitude was computed as

$$\hat{\alpha}_n(\omega) \equiv \mathcal{F}[|\alpha_n(t)|^2], \quad (11)$$

where  $\mathcal{F}$  stands for the Fourier transform. The spectra are the main targets that we address, aiming to observe the effect of the potential in the underlying GPE, as motivated by Fig. 1. To produce  $\hat{\alpha}_n(\omega)$ , we solve Eq. (2) numerically, using the schemes outlined in Appendix A, and then identify amplitudes  $\alpha_n(t)$  as per a truncated version of Eq. (10).

As initial conditions we use waves prepared with random phases and amplitudes, in the form of

$$\alpha_n(0) = \begin{cases} \mathcal{A}_n e^{i\mathcal{P}_n} & \text{for } n \leq \mathcal{N}, \\ \mathcal{A}_n e^{i\mathcal{P}_n} e^{-\beta(n-\mathcal{N})} & \text{for } n > \mathcal{N}, \end{cases} \quad (12)$$

where  $\mathcal{A}_n$  and  $\mathcal{P}_n$  are random numbers uniformly distributed in intervals  $[0,1]$  and  $[0, 2\pi)$ , respectively,  $\mathcal{N}$  is the number of significantly excited modes, and  $\beta > 0$  determines the suppression of higher modes. The value of  $M$  is not fixed by

$\mathcal{N}$  and  $\beta$  in Eq. (12). For this reason, the set of initial amplitudes  $\alpha_n(0)$  is scaled to satisfy the normalization,  $M = 1$ . We use input (12) because the exponential suppression of the higher modes typically occurs in configurations arising in the course of the dynamical evolution. Each realization of input (12) features a different content of modes and phases, yielding an adequate form of generic (“natural”) initial states. Therefore, they provide an appropriate arena for formulating generic results. This approach brings in a broader perspective in comparison with focusing on special solutions, such as single solitons. In this regard, our simulations may actually be understood as the evolution of configurations given by superpositions of a large number of dark solitons, corresponding to notches in the pattern (the superposition also including other ingredients), as Fig. 2 suggests.

Random initial conditions similar to those defined by Eq. (12) are used in studies of the wave turbulence [78], with the aim to produce a generic dynamical picture, rather than focusing on specific solutions. In particular, the 1D NLSE in a very broad box with periodic boundary conditions was used to study the dynamics of random waves in integrable equations [79–81] (implementing the concept of the “integrable turbulence” introduced by Zakharov [82]), the formation of rogue waves [83–85], etc. Initial conditions of the same type have been also used in the context of the 2D NLSE with a truncated HO potential in connection with experiments on the light propagation in multimode optical fibers [86–90], and in general, in the studies of optical wave turbulence [91]. Thus, our use of random initial configurations in the presence of trapping potentials follows the general framework adopted for the studies of spatially confined random waves.

A detailed visualization of the evolution of random waves in the HO and box potentials is produced, respectively, in the left and right columns of Fig. 2. In both cases, the evolution is affected by the nonlinearity and broad wavelength spectrum of the initial excitation ( $g = 250$ ,  $\mathcal{N} = 20$ ,  $\beta = 1$ ).

Proceeding with the analysis, we first dwell on the case of the HO potential. In this case, profile  $|\psi(x)|$  is initially localized at the center of the domain, exhibiting many notches. At the initial stage of the subsequent evolution, the profile performs a sequence of alternating expansion-compression cycles under the action of the HO potential [Fig. 2(Ia)], and then relaxes to a spread state [Fig. 2(Ib)] that keeps a nearly constant envelope in time, together with a large number of notches shuttling from side to side, resembling a gas of dark solitons [92]. The relaxation process may be observed in Fig. 2(Ic) in the evolution of the energy terms  $H_2$  and  $H_4$ , defined as per Eqs. (5) and (6). Their ratio, starting from  $H_4/H_2 \approx 2.2$  [inset in Fig. 2(Ic)], initially oscillates with large amplitudes corresponding to expansion and compression of the profile. After  $t \approx 80$  the energy exchanges significantly subside, with the energies oscillating around nearly constant values in the course of the subsequent evolution, with the ratio  $H_4/H_2 \simeq 0.42$ , which is essentially larger than in the weakly nonlinear regime ( $H_4/H_2 \ll 1$ ). The power spectrum associated with this evolution scenario features, in Fig. 2(Ie), a comblike shape similar to that exhibited above in Fig. 1(a). While one might assume that this shape originates from the initial expansion-compression stage, the simulations are long

enough to guarantee the completion of the system’s relaxation in the course of 20% of the total simulation time, while the established stage of the evolution covers the remaining 80% of the time. Moreover, omitting the initial relaxation stage in the computation of the power spectrum, its shape practically does not change. The same happens if one performs extremely long simulations, which also reveal the establishment of a comblike structure, see (Appendix C). As concerns the propagation of dark solitons in the profile, Figs. 2(Ia) and 2(Ib) exhibit their relatively smooth trajectories at both stages of the evolution, the expansion-compression and established ones.

In the case of the box potential, Fig. 2(II) shows that the random-phase-and-amplitude input (12) fills the box from the beginning, remaining in this state at all times. We have also explored the case where the random-phase-and-amplitude input is localized at the center of the box. In that case, following the initial expansion, the profile remains in the spread state, without featuring expansion-compression cycles. In the course of the evolution, the energies again keep the ratio  $H_4/H_2 \simeq 0.42$ . Taking close-by values of this ratio in the cases of the HO and box potentials is necessary, once the objective is to compare similar nonlinear regimes. In spite of the proximity of the ratio  $H_4/H_2 \simeq 0.42$  in both cases, the action of the box potential leads to the emergence of a continuous (ergodic) power spectrum in Fig. 2, in contrast with its comb-shaped counterpart for the HO potential. It is also worthy to note a significant difference in the range of excited frequencies in the respective power spectra. We stress that the difference from the case of the HO potential is not a mere consequence of the mismatch in the box size, because we have set  $L = \pi/\sqrt{2}$  above precisely with the purpose to match the linear energy spectra of both systems [ $(E_n)_{\text{HO}} = n + 1/2$  and  $(E_n)_{\text{box}} = (n + 1)^2$ ], and, as we show in the next section, this value of  $L$  provides matching of positions of the excited frequencies in the power spectra of both systems. The ergodicity in case of the box-shaped potential has been previously observed in Ref. [27] for initial conditions that expand from the center, in agreement with our inference that there is no essential difference from the long-time evolution initialized by the input filling the entire domain. Similar to the HO potential, it is observed that dark solitons propagate throughout the box, but they do not follow smooth trajectories even in its interior, because of multiple collisions between them, and shapes of individual solitons are identified less clearly than in the case of the HO potential

We have also tested the presence of ergodicity in the case of non-HRPs whose generically shaped spectra of energy eigenvalues do not admit resonances. For instance, the 1D quartic potential,  $V(x) = x^4/2$ , is a non-HRP one, as shown by lowest eigenvalues numerically computed with accuracy  $\Delta E_n \sim 10^{-4}$ :

$$\begin{aligned} E_0 &= 0.5302, & E_1 &= 1.8998, & E_2 &= 3.7278, \\ E_3 &= 5.8224, & E_4 &= 8.1309, & E_5 &= 10.6192, \\ E_6 &= 13.2642, & E_7 &= 16.0493, & E_8 &= 18.9615. \end{aligned} \quad (13)$$

In this case, the input provided by random waves gives rise to an initial expansion-compression stage before

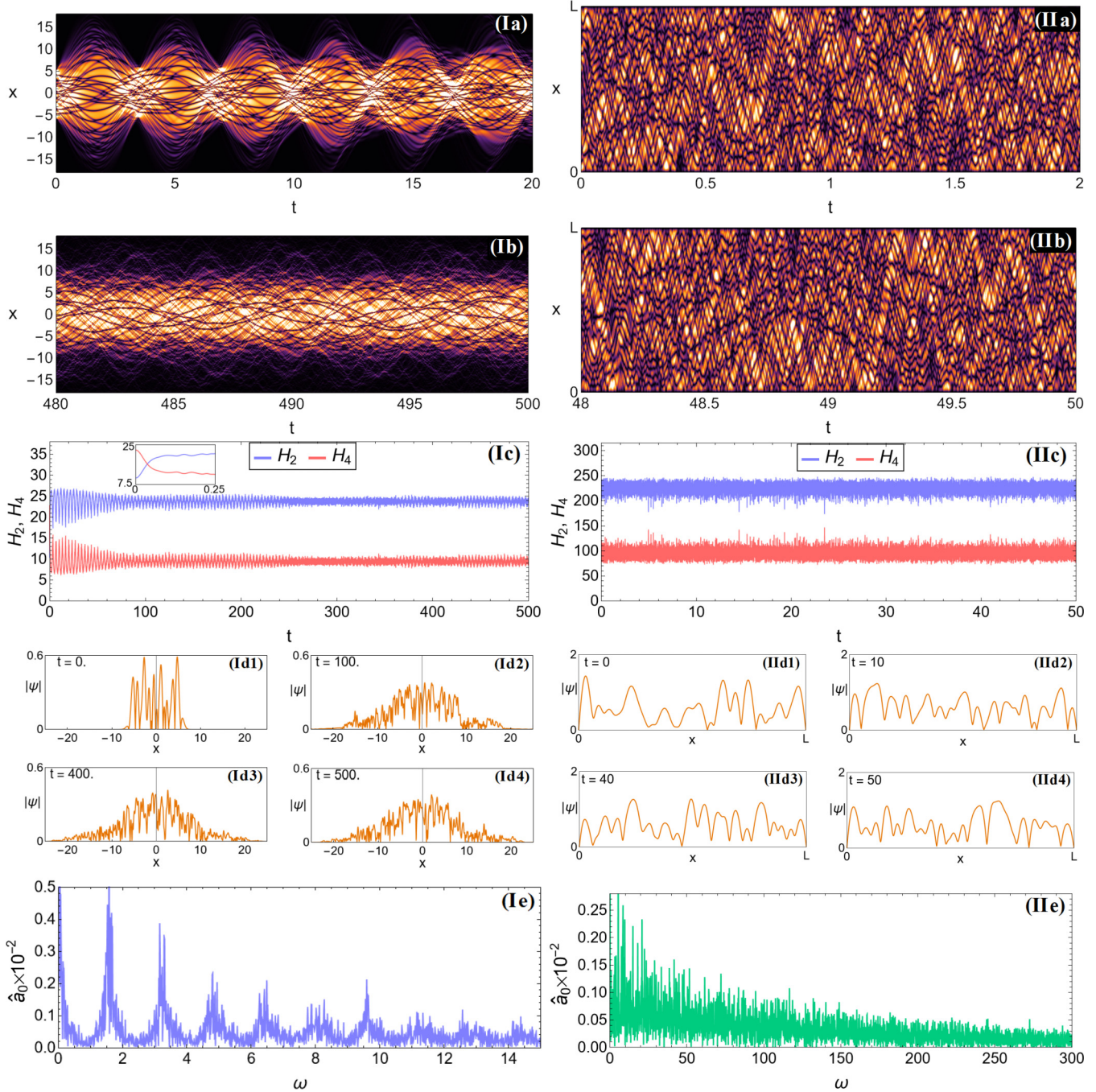


FIG. 2. The evolution of 1D defocusing random waves under the action of the HO (left column, labeled I) and box-shaped potentials of size  $L = \pi/\sqrt{2}$  (right column, labeled II), for a large nonlinearity coefficient  $g = 250$  in Eq. (2). From top to bottom: the initial stage of the spatiotemporal evolution (a); the evolution at an advanced stage (b); the temporal evolution of the quadratic (5) and quartic (6) parts of the energy (c); four snapshots illustrating the shape of the profile in the course of the evolution (d); and the power spectrum of the lowest-mode’s amplitude,  $\alpha_0(t)$  (e), with higher modes displaying similar shapes. The initial conditions are random waves prepared as per Eq. (12) with  $\mathcal{N} = 20$  and  $\beta = 1$ . Both cases, corresponding to the HO and box potentials, keep the ratio  $H_4/H_2 \simeq 0.42$  at the established stage of the evolution.

relaxing to a spread state, apparently similar to the dynamical scenario observed above under the action of the HO potential, but the power spectrum is ergodic in the present case, see Fig. 1(c), like in the case of the box potential, cf. Fig. 2(IIe), in agreement with the general picture outlined above.

### III. THE ANALYTICAL DESCRIPTION IN THE WEAKLY NONLINEAR REGIME

In this section, we aim to provide an analytical form of the power spectrum in the weakly nonlinear regime, with  $|g| \ll 1$  in Eq. (2), in which the difference in the emergence

of comblike or ergodic spectra in HRP and non-HRP can be understood explicitly. To do that, we again address the 1D GPE with the HO and box potentials, which generate, as mentioned above, the following commonly known equidistant and quadratic spectra:

$$\text{HO: } E_n = n + \frac{1}{2}; \quad \text{box: } E_n = \frac{\pi^2}{2L^2}(n+1)^2. \quad (14)$$

First, we are going to demonstrate that both potentials produce, in the case of weak nonlinearity, a comblike power spectrum composed of “slender” peaks. After that, we show how the eigenvalues determine interactions between the eigenmodes, and how the equidistant eigenvalues in the case of the HO potential arrange the interactions in a way that helps to preserve the comblike spectrum as the nonlinearity strengthens. However, we demonstrate that the deviation from the equidistant structure of the spectrum in the case of the box potential is responsible for erasing the comblike spectral shape, already for moderately weak nonlinearity. The extension of the analysis to generic HRP subject to condition (1) is presented in Appendix B, where we show that our arguments developed for the HO potential apply to generic HRP as well, safeguarding the preservation of the comblike power spectra. The arguments are independent of the sign of  $g$ , thus being valid for both the defocusing and focusing signs of the nonlinearity. For this reason,  $g$  means  $|g|$  in this section.

### A. Slender comblike spectrum

For our analysis, it is useful to rewrite the 1D GPE (2) as a system of equations for mode amplitudes  $\alpha_n$ . To do that, one has to insert  $\psi(t, x)$ , written in the form of expansion (10), in Eq. (2), and project the result onto eigenmodes  $f_n(x)$ . This results in a system of ordinary differential equations for the evolution of the amplitudes,

$$i \frac{d\alpha_n}{dt} = g \sum_{m=0}^{\infty} \sum_{i=0}^{\infty} \sum_{j=0}^{\infty} C_{nmij} \bar{\alpha}_m \alpha_i \alpha_j e^{i\Delta_{nmij}t}, \quad (15)$$

where the bar stands for the complex conjugate,

$$\Delta_{nmij} \equiv E_n + E_m - E_i - E_j \quad (16)$$

are the resulting frequencies of the four-wave interaction, and with the respective couplings constants,

$$C_{nmij} = \int_{-\infty}^{+\infty} f_n(x) f_m(x) f_i(x) f_j(x) dx. \quad (17)$$

Expressions (15)–(17) are valid for any trapping potential, including the HO and box ones, the distinction being in the values of  $\Delta_{nmij}$  and  $C_{nmij}$ , when one inserts specific eigenvalues  $E_n$  and eigenmodes  $f_n(x)$  into the expressions.

Using Eq. (15), we aim to demonstrate, first, that the structure of the power spectrum is quite simple for the weak nonlinearity ( $g \ll 1$ ). The equations give rise to two constituents of the evolution, as seen in Fig. 3. On the one hand, there are frequencies  $\sim g$  and amplitudes  $\sim 1$ , which are associated with resonances. On the other hand, there are contributions with small amplitude  $\sim g$  corresponding to frequencies associated with nonresonant interactions. The frequencies of the latter type are precursors of the characteristic

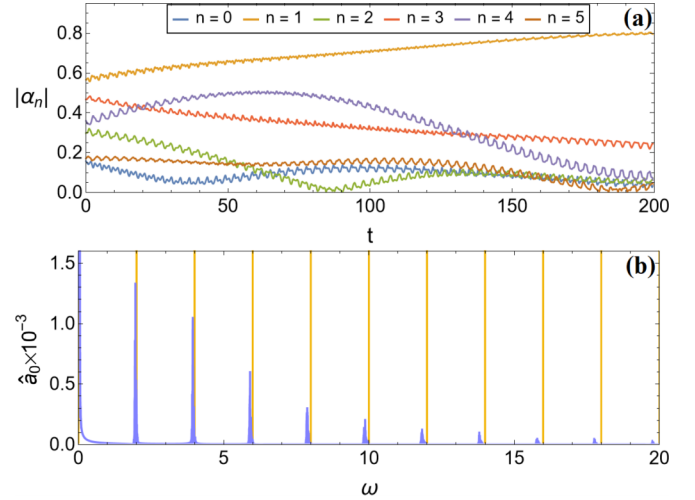


FIG. 3. The evolution of  $\alpha_n$  (a) and power spectrum of  $|\alpha_0|^2$  (b) governed by the 1D GPE with the HO potential and defocusing sign of the nonlinearity. In panel (a) two constituents of the evolution are observed: long-time modulations and small-amplitude oscillations, which are associated with resonant and nonresonant interactions, respectively. In panel (b) the effect of these terms on the power spectrum of  $|\alpha_0|^2$  is observed. Vertical yellow lines mark our analytic prediction,  $\mathcal{W}_{2k} = 2k$ , for the location of the excited frequencies in the case of the weak nonlinearity [see Eq. (19)], which demonstrates very accurate agreement, up to a slight shift originating from nonlinear corrections. These numerical results were produced for  $g = 1$ , to comprise the slow and fast constituents in the evolution of  $\alpha_n$  in the framework of the same plot. The picture demonstrates that the analytical prediction, originally obtained for  $g \ll 1$ , works very well in this case too.

spikes in the comblike spectrum which exist in the case of strong nonlinearity, as shown in the next section. In view of their relevance to the analysis, we introduce them by means of the following.

*Definition.*  $\mathcal{W}_k$  with  $k \in \mathbb{Z}$  represent all different values of  $\Delta_{nmij}$  with  $n, m, i, j \in \mathbb{N}$ , defined by Eq. (16), and arranged in the increasing order,

$$\dots < \mathcal{W}_{k-1} < \mathcal{W}_k < \mathcal{W}_{k+1} < \dots \quad \text{with } k \in \mathbb{Z}. \quad (18)$$

When  $\Delta_{nmij}$  take the same value for different sets of the indices, there is single  $\mathcal{W}_k$  associated with that value (for instance,  $\Delta_{nmnn} = 0$  for any  $n$ , hence there is single  $k$  for which  $\mathcal{W}_k = 0$ ).

For generic systems, eigenvalues  $E_n$  are irrational numbers, hence frequencies  $\mathcal{W}_k$  may form sets which are denser than the underlying sets of eigenvalues  $E_n$ . As one proceeds to stronger nonlinearity, further combinational harmonics arise, filling in frequency axis still denser and leading to the emergence of generic continuous power spectra. The situation is much more subtle for systems with integer eigenvalues  $E_n$ , as is the case for the HO and box potentials, since  $\mathcal{W}_k$  are then integers too. In this case, further analysis is required to identify the shape of the power spectra, which arises from the effect of the right-hand side (RHS) of Eq. (15) on the evolution of  $\alpha_n$ . In the present context, two key ingredients are prefactor  $g$  and the complex exponential, which is an oscillatory term with frequency  $\Delta_{nmij}$  that vanishes in the

resonant case,  $\Delta_{nmij} = 0$ . When  $g$  is very small, the evolution splits in components corresponding to the natural timescales,  $t \sim \mathcal{O}(1)$ ,  $\mathcal{O}(1/g)$ , etc. [93,94]. For  $t \sim \mathcal{O}(1)$ ,  $\alpha_n$  remain constant up to nonlinear contributions of orders  $\sim g$  and higher. We focus on the contributions of order  $g$  because they dominate in this regime. On the one hand, resonant terms with  $\Delta_{nmij} = 0$  generate contributions  $\sim gt$  (i.e., secular terms in terms of the “naive expansion” in powers of  $g$ ), which induce substantial modulations in  $\alpha_n$  at times  $t \sim \mathcal{O}(1/g)$  (see the slow evolution of  $|\alpha(t)|$  in Fig. 3). Therefore, such long-time modulations excite frequencies  $\sim g$  in the power spectrum. On the other hand, nonresonant terms, with  $\Delta_{nmij} \neq 0$ , oscillate with frequencies  $\Delta_{nmij}$  (including corrections  $\sim g$ ) and amplitudes  $\sim g$  (see small oscillations of  $|\alpha(t)|$  in Fig. 3). The latter terms excite frequencies  $\Delta_{nmij}$  in the power spectrum of  $\alpha_n$  (with corrections  $\sim g$ ), and have amplitudes  $\sim g$ . From here, we conclude that the structure of the power spectrum in the weakly nonlinear regime includes two kinds of excitation frequencies: those determined by  $\mathcal{W}_k$ , and the frequencies forming a continuum in a small region of width  $\sim g$  around the origin. When the nonlinearity strength grows, frequencies produced as combinations from these two sets will emerge, being responsible for the broadening of the sharp peaks located at various values of  $\mathcal{W}_k$ .

From the previous discussion, one can deduce the condition to display the comblike power spectrum in the regime of weak nonlinearity. This is just the condition that  $\mathcal{W}_k$  must be equidistant because the spectrum is tightly localized around  $\mathcal{W}_k$ . The 1D GPE with the HO and box potentials precisely satisfy this property because they give rise to

$$\mathcal{W}_{2k} = 2k \quad (19)$$

and  $\mathcal{W}_{2k} = \pi^2 k/L^2$ , respectively. This means that both potentials give rise to a “slender” version of the comblike power spectrum in the case of very weak nonlinearity. The expressions for  $\mathcal{W}_{2k}$  follow from Eqs. (14) and (16),

$$\Delta_{nmij} = (n + m - i - j) \quad \text{with} \quad n, m, i, j \in \mathbb{N}, \quad (20)$$

$$\Delta_{nmij} = \frac{\pi^2}{2L^2} [(n+1)^2 + (m+1)^2 - (i+1)^2 - (j+1)^2], \quad (21)$$

in the case of the HO and box potential, respectively. To make the structure of expression (21) more transparent, we set  $m = i - 1$ ,  $j = n - 1$ , which yields  $\Delta_{nmij} = \pi^2(n - i)/L^2$ , so that any integer is generated at times  $\pi^2/L^2$ . We use index  $2k$  in Eq. (19), instead of  $k$ , to highlight the absence of interactions between three modes with odd numbers and an even one, and vice versa, for parity reasons [the respective couplings  $C_{nmij}$  vanish according to Eq. (17), hence  $\mathcal{W}_{2k+1}$  are not present in the power spectrum]. To ensure a meaningful comparison between the HO and box potentials, we choose, as said above,  $L = \pi/\sqrt{2}$ . Then, the spike positions ( $\mathcal{W}_{2k}$ ) in the power spectrum are the same for the two cases in the weakly nonlinear regime. By means of such identification of the frequency scales, a meaningful comparison is possible between the HO and box-shaped potentials also for strong nonlinearity.

## B. Departing from the weakly nonlinear regime

It has been demonstrated above that the 1D GPE with the HO or box potentials display a comblike power spectrum for very weak nonlinearity. However, as Figs. 1 and 2 show, this shape of the spectrum is not preserved in the case of the box-shaped potential, turning into a generic ergodic spectrum with the increase of the nonlinearity strength. Here, we aim to explain why, nevertheless, the HO potential preserves the comblike shape of the power spectrum even for strong nonlinearity. We demonstrate that the key difference is due to the linear and quadratic eigenvalue spectra (14) of these systems. This is because the eigenvalues determine, through the frequency combinations  $\Delta_{nmij}$ , which modes are involved in the four-wave interactions, and then different structures of  $\Delta_{nmij}$  in Eqs. (20) and (21) produce different predictions for the excitation of frequencies  $\mathcal{W}_k$ . We show that, through this mechanism, equidistant eigenvalues produce a strong suppression of large frequencies, while a large range of them are excited in case of the quadratic eigenvalue spectrum in Eq. (14).

To demonstrate this, one has to estimate the contribution of the  $k$ th frequency  $\mathcal{W}_k$  to the  $n$ th mode  $\alpha_n$ . For that purpose, one gathers all terms oscillating with frequency  $\mathcal{W}_k$  on the RHS of Eq. (15), writing the system of equations as

$$i \frac{d\alpha_n}{dt} = g \sum_{k=-\infty}^{\infty} \mathcal{S}_n(k) e^{i\mathcal{W}_k t}, \quad (22)$$

$$\mathcal{S}_n(k) \equiv \underbrace{\sum_{m=0}^{\infty} \sum_{i=0}^{\infty} \sum_{j=0}^{\infty} C_{nmij} \bar{\alpha}_m \alpha_i \alpha_j}_{\Delta_{nmij} = \mathcal{W}_k} \quad (23)$$

The “sources”  $\mathcal{S}_n(k)$  defined by Eq. (23) determine the contribution of the  $k$ th frequency  $\mathcal{W}_k$  to the  $n$ th mode  $\alpha_n$ . Numerical computations using values of  $\alpha_n$  extracted from our simulations reveal that  $\mathcal{S}_n(k)$  decay with  $|k|$  considerably faster for the HO potential than the for its box-shaped counterpart, as Fig. 4 shows (except for a few values of  $k$  as, explained below). This picture is confirmed analytically in Appendix B showing that the amplitudes  $\mathcal{S}_n(k)$  decay exponentially in the former case,

$$|\mathcal{S}_n(k)_{\text{HO}}| < e^{-\beta|k-n|} P_{n,k}, \quad (24)$$

while they exhibit a much slower decay for the box-shaped potential,

$$|\mathcal{S}_n(k)_{\text{box}}| < e^{-\beta\sqrt{|k-(n+1)^2|}} D_{n,k}, \quad (25)$$

where  $P_{n,k}$  and  $D_{n,k}$  are polynomials in  $n$  and  $k$ , and  $\beta$  is a positive constant. To derive these results, we have used a “phenomenological” analytical constraint for  $\alpha_n$  that captures the qualitative structure revealed by our simulations, see Fig. 4(c),

$$|\alpha_n| < p_n^{(s)} e^{-\beta n} \mathcal{A}_n, \quad (26)$$

where  $\beta > 0$  is the same constant as in Eqs. (24) and (25),  $p_n^{(s)}$  is a polynomial of degree  $s \geq 0$ , while  $\mathcal{A}_n$  is a random variable uniformly distributed in the interval of  $[0,1]$ .

Below, we explain that the difference between the HO and box potentials in the decay of  $|\mathcal{S}_n(k)|$  with  $k$  has an impact on the structure of the power spectrum in the cases of weak and

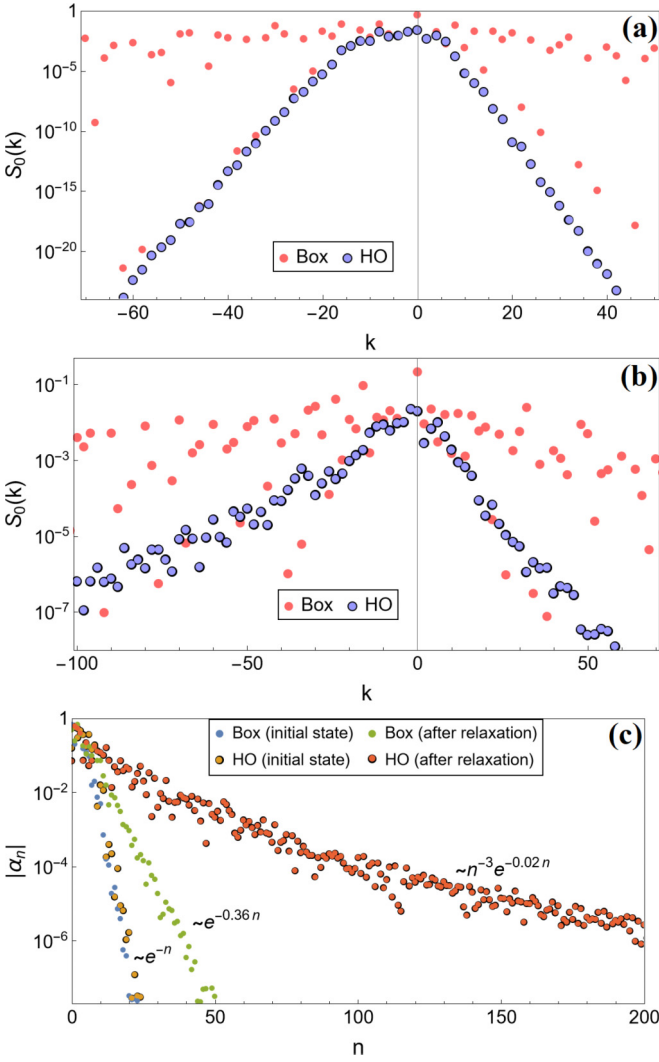


FIG. 4. The dependence of amplitude  $\mathcal{S}_0(k)$  on  $k$  in the cases of the HO and box potentials, as produced by the numerical solutions initialized by input (12) with random phases and amplitudes, for  $\mathcal{N} = 5$  and  $\beta = 1$ . (a)  $\mathcal{S}_0(k)$ , associated with the initial state, when  $\alpha_n$  feature the exponential decay  $\sim e^{-n}$  in both systems. (b) The same amplitudes after the relaxation of the systems, when  $\alpha_n$  demonstrate a stronger suppression with  $n$  in the box ( $\sim e^{-0.36n}$ ) than in the case of the HO potential ( $\sim n^{-3}e^{-0.02n}$ ), while  $\mathcal{S}_0(k)$  still decay faster in the latter case. (c) Values of  $|\alpha_n|$  used in panels (a) and (b).

moderate nonlinearities, but, prior to that, we should clarify where this difference comes from. One might conjecture that it is associated with the couplings  $C_{nmij}$ , but the actual reason is the difference between the equidistant (8) and quadratic (9) energy spectra, together with the rapid decay of  $\alpha_n$  (26). As we show in Appendix B, for HRP's satisfying condition (1), such as the HO potential, and  $\alpha_n$  given by Eq. (26),  $\mathcal{S}_n(k)$  decays exponentially for large  $|k|$ , independent of whether  $C_{nmij}$  decay, remain constant, or grow with the increase of the indices, while the quadratic spectrum, such as the one corresponding to the box potential, features a much slower decay. The key point is in the restriction on the indices necessary to get  $\Delta_{nmij} = \mathcal{W}_k$  in Eq. (23). Namely, fixing  $k$ , the modes involved in the interactions that generate frequency

$\mathcal{W}_k$  differ for the spectra (20) and (21). In the former case, large  $k$  requires at least one high-order mode involved, while in the latter case the quadratic eigenvalues make it possible to achieve large  $k$  easier, using low-order modes in most cases.

Thus, the exponential decay of high modes gives rise to the difference in the magnitude of  $\mathcal{S}_n(k)$ . The following examples illustrate this picture (Example I), and also explain the strong decay of some amplitudes  $\mathcal{S}_n(k)$  observed in the box in Fig. 4 (Example II).

*Example I.* Frequency  $\mathcal{W}_{35}$  contributes to  $\alpha_0$  via several combinations of modes  $\{n, m, i, j\}$  in Eq. (23). For the sake of simplicity we use the following expressions in this example:

$$\alpha_n = e^{-n}, \quad \text{and} \quad C_{nmij} = 1, \quad (27)$$

while the conclusion is the same for other choices of  $\alpha_n$  and  $C_{nmij}$ , as explained in Appendix B. We focus on the largest contributions to  $\mathcal{S}_0(35)$ , which involves the lowest possible modes,  $\{0, 35, 0, 0\}$  in the case of the HO spectrum (20), or  $\{0, 5, 0, 0\}$  in the case of the box spectrum (21). Then, it follows from Eq. (23) that the contribution of this interaction in the case of the HO potential,  $\bar{\alpha}_{35}\alpha_0\alpha_0 = e^{-35}$ , is many orders of magnitude smaller than the one in the case of the box potential,  $\bar{\alpha}_5\alpha_0\alpha_0 = e^{-5}$ , because they, respectively, involve modes  $m = 35$  and  $m = 5$  to generate the same frequency  $\mathcal{W}_k$ .

*Example II.* Reproducing the previous example, but with frequency  $\mathcal{W}_{38}$  instead of  $\mathcal{W}_{35}$ , one finds that the largest contribution to  $\mathcal{S}_0(38)$  in the box, ( $\bar{\alpha}_{20}\alpha_1\alpha_{19} = e^{-40}$ ), is close to its counterpart in the case of the HO potential ( $\bar{\alpha}_{38}\alpha_0\alpha_0 = e^{-38}$ ). This difference from the common situation (see Fig. 4) happens because there are no relatively low-order modes that satisfy condition (21) for special combinations of  $(n, k)$ . This is the explanation behind the strong suppression of a few amplitudes  $\mathcal{S}_0(k)$  in the box observed in Fig. 4. No essential contribution from these amplitudes is expected in the subsequent description of the population of the power spectrum because of their low presence and small values.

For weak nonlinearity, the difference in the decay of amplitudes  $\mathcal{S}_n(k)$  corresponding to the HO and box potentials has an impact on the power spectrum because they determine the excitation of frequencies  $\mathcal{W}_k$ . The strong suppression of  $\mathcal{S}_n(k)$  in the HO case is translated into strong suppression of high frequencies  $\mathcal{W}_k$  (rapid decay of peaks in the comblike power spectrum), while the much slower suppression of  $\mathcal{S}_n(k)$  in the case of the box potential facilitates excitation of higher frequencies (observed as spectral peaks at higher frequencies). In the regime of moderate nonlinearity, amplitudes  $\mathcal{S}_n(k)$  have an even stronger influence on the shape of the power spectrum, as we aim to explain now. In this regime, the evolution of  $\alpha_n$  no longer features solely two motions contributed to by resonances ( $\Delta_{nmij} = 0$ ) and oscillations with frequencies  $\mathcal{W}_k$ , like in Fig. 3(a), as subdominant oscillatory terms start to appear as relevant ones. Thereby, the equidistant structure of  $\mathcal{W}_k$  is no longer sufficient to maintain the comblike spectrum. Subdominant components emerge from the combination of the resonant and nonresonant terms, as mentioned above. Namely, these combined terms act as sources driving the generation of subdominant components (similar to the usual principle that, in any perturbative expansion, higher-order terms are sourced by lower-order ones). Frequencies of the terms that emerge in this way result from combinations of  $\mathcal{W}_k$  and those  $\sim g$

around the origin. They produce contributions in the power spectrum that slightly deviate from  $\mathcal{W}_k$ , broadening in this way the “slender” spikes in the power spectrum in the weak-nonlinearity regime. This set of subdominant contributions is naturally extended to higher orders in  $g$ , producing more and more frequencies in the power spectrum which are originally sourced by  $\mathcal{S}_n(k)$ . Therefore, the behavior of these amplitudes determines how the power spectrum is populated when the system departs from the weakly nonlinear regime. In the case of the box potential, we have demonstrated above that  $\mathcal{S}_n(k)$  slowly decay with  $|k|$  [see Eq. (25)], thus giving rise to a broad range of high frequencies  $\mathcal{W}_k$ , and triggering the rise of a large number of high-frequency subdominant peaks, which dress the basic power spectrum with a complicated structure. In this way, the comblike spectral shape, which persists in the weakly nonlinear regime, quickly gets destroyed, a spectral tail of high frequencies arises, and individual peaks broaden considerably, absorbing multiple combinational contributions arising from already excited peaks. In the case of the HO potential, higher-order contributions are, of course, produced as well, but the exponential suppression of high-frequencies  $\mathcal{W}_k$ , as seen in Eq. (24), ensures that a majority of subdominant terms are suppressed as well. This mechanism drastically reduces the number of significant subdominant contributions the power spectrum receives, preventing its “wild” population and protecting its comblike structure. Note that, while our analysis is performed in the framework of the weakly nonlinear regime, the picture produced by it correctly captures the shapes of the power spectra for the strong nonlinearity, as observed in Figs. 1 and 2: a disordered distribution of many spikes in the case of the box-shaped potential, and the nearly equidistant array of spikes in the HO case, confined to the low-frequency range.

Before concluding the analysis of the weakly nonlinear regime, we aim to highlight differences between the present analysis and works on quasiperiodic solutions and FPU recurrences in the 2D GPE with the HO potential. In both cases, the modal decomposition (15) has been used, but Refs. [67,69,70] focused on resonant interactions, namely, long-time dynamics at  $|g| \ll 1$ , exploiting the specific structure of  $C_{nmij}$  and neglecting nonresonant interactions. However, our analysis considers both resonant and nonresonant interactions, while the specific form of  $C_{nmij}$  for each system was not used. It was done with the purpose of getting a description of the power spectrum of HRP in the weakly nonlinear regime, that helps to guide the intuition for moderate values of  $|g|$ . It is worth mentioning that analytic solutions obtained in Refs. [67,69] are not generic among the class of HRP, as they rely on a special structure of  $C_{nmij}$  [71,72], although they have a significant presence in the class of NLSEs [67,69,72,75,95]. However, a part of the study of FPU recurrences performed in [70] relied on less restrictive property of  $C_{nmij}$ , leaving open the possibility that this kind of dynamics is generic for NLSEs with HRP.

#### IV. NUMERICAL RESULTS IN THE FULLY NONLINEAR REGIME

Having explained the emergence of the comblike power spectra for weak nonlinearity, it is natural to explore how the

picture changes toward strong nonlinearity. Specifically, it is relevant to find out how the structure gradually deviates from the above prediction for the weakly nonlinear regime with the increase of  $|g|$ , and how it depends on the sign of the nonlinearity, self-defocusing ( $g > 0$ ) or focusing ( $g < 0$ ).

Figure 5 provides answers to these questions. One observes how the comblike spectrum evolves away from the “slender” version as the nonlinearity strength grows, for the 1D GPEs with the box and HO potentials. The comparison between these potentials demonstrates that the main predictions of the weakly nonlinear analysis developed above still hold qualitatively in the fully nonlinear regime. The power spectrum for the box potential transits from the comblike shape to an ergodic one, which includes a conspicuous high-frequency component. However, the spectrum corresponding to the HO potential still keeps a comblike spectral shape for large values of  $|g|$ . This contrast between the different potentials reflects the fact that the equidistant linear energy spectrum (1) plays a central role in the strongly nonlinear regime too. Nevertheless, these results are not explained by proximity to the linear regime. Indeed, while the “slender” power spectra exist at small  $g$  in both cases of the HO and box potentials, extending them to a comparable level of the nonlinearity, characterized by the ratio  $H_4/H_2$  of the energy terms, see Eqs. (5) and (6), the GPE with the HO potential still maintains a comblike spectrum, while its counterpart with the box potential displays an ergodic spectral distribution, totally different from the weakly nonlinear regime.

For the case of the HO potential in the GPE with focusing and defocusing nonlinearities, Fig. 5 shows two characteristic effects involving spikes of the comblike spectra. The first is a gradual deviation from locations  $\mathcal{W}_k$ , that were predicted in the weak-nonlinearity regime, toward smaller (larger) frequencies for the defocusing (focusing) sign of the nonlinearity (in agreement with the usual definitions of the self-defocusing and focusing), while keeping their nearly equidistant structure. The second effect, observed with the growth of  $|g|$ , is that the spectral spikes get wider, and at some point they start to overlap with each other, compromising the comblike shape. The magnitude of  $|g|$  at which this happens depends on the sign of the nonlinearity. In the case of the self-attraction, the transition happens at much lower values of  $|g|$ . This trend can be easily explained too, noting that the focusing nonlinearity enhances the interaction and mixing between different modes, while the defocusing suppresses the interaction.

Note that the above analysis is presented for the nonlinearity magnitude,  $g$ , treated as the control parameter. An alternative way to quantify the strength of the nonlinearity is, as mentioned above, to use the ratio between the quadratic and quartic energies,  $|H_4|/H_2$ . We observe that, with the increase of  $|g|$ , the self-focusing GPE rapidly accumulates energy in the nonlinear terms, which is translated into larger values of  $|H_4|/H_2$ , in comparison to the defocusing case, which requires much higher values of  $g$  to reach the same ratio.

The transition from the comblike power spectrum to ergodicity in the case of very strong nonlinearity is not surprising. What is nontrivial in these results, is the great impact the equidistant structure of the linear spectrum on the nonlinear regime and the persistence of the nonergodic spectrum even for strong nonlinearity.

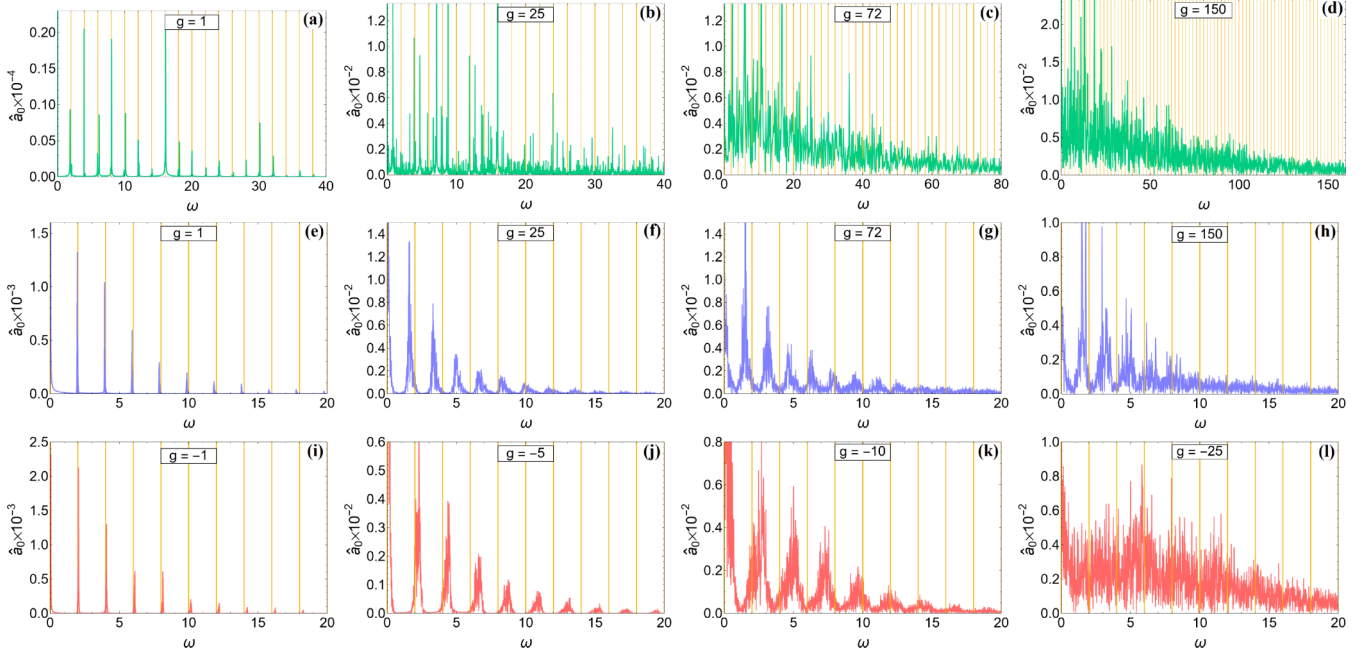


FIG. 5. The power spectrum produced by the defocusing 1D GPE with the box-shaped potential (a)–(d), and by the defocusing and focusing [(e)–(h) and (i)–(l), respectively] 1D GPE with the HO potential. The computations of the spectra for increasing values of the nonlinearity strength,  $|g|$ , are performed with random-wave initial conditions. The initial data are the same for all plots in the case of the HO potential. Vertical yellow lines mark the location of  $\mathcal{W}_{2k}$ , see Eq. (19).

## V. OTHER NONLINEAR SCHRÖDINGER EQUATIONS WITH HRPS (HIGHLY RESONANT POTENTIALS)

In the above analysis, we addressed the 1D GPE with the HO potential as the guiding example to present the characteristic features of HRPs and observe how their resonance structure hinders the onset of the ergodicity. Here, we proceed to demonstrate that this effect is generic for other resonant potentials, which cover a wide range of interesting models. To this end, we have explored the dynamics of NLSEs with different nonlinearities, including HRPs in different spatial dimensions, a two-component NLSE, and even a relativistic wave equation. Below, we present detailed results for these equations. In Fig. 6, one can see that all of them display comblike power spectra, confirming the genericity of the principles formulated above. Actually, these findings imply that the form of the nonlinearities plays a secondary role, as it determines the values of  $g$  at which comblike spectra transit to ergodic ones, but not the overall presence of the effect.

### A. The quintic 1D NLSE with the HO potential

A natural modification of the original 1D GPE with the HO potential is to replace the cubic nonlinear term by the quintic one. The equation has the form

$$i\partial_t \psi = -\frac{1}{2}\partial_{xx}\psi + \frac{1}{2}x^2\psi + g|\psi|^4\psi, \quad (28)$$

keeping the equidistant spectrum,  $E_n = n + 1/2$ . This modification provides a new setting because the cubic 1D NLSE in the free space is integrable, while the quintic one is not, and gives rise to 1D Townes solitons and critical collapse [96]. This, in particular, rules out the integrability of the underlying equation in the free space as a reason for the emergence of

comblike power spectra. With  $t$  replaced by the propagation distance,  $z$ , Eq. (28) is a natural model for a planar waveguide in optics, where the purely quintic nonlinearity may be realized in colloidal suspensions of metallic nanoparticles [97].

### B. D-dimensional cubic and quintic NLSEs with the HO potential

It is also natural to explore the existence of comblike power spectra in higher dimensions (here we restrict the consideration to the case of spherical symmetry). We did that for the cubic and quintic NLSEs with the HO potential:

$$i\partial_t \psi = \frac{1}{2}\left(-\partial_{rr} - \frac{D-1}{r}\partial_r + r^2\right)\psi + g|\psi|^{p-1}\psi, \quad (29)$$

where  $r \in [0, \infty)$  is the radial coordinate,  $D = 2, 3, \dots$  is the spatial dimension, and  $p = 3$  or  $5$  is the power of the nonlinear term. For any combination of these parameters and  $g > 0$  (self-repulsion, otherwise the multidimensional NLSE gives rise to the collapse [98]), Eq. (29) has the commonly known equidistant linear energy spectrum of the multidimensional HO,  $E_n = 2n + d/2$ .

### C. Anharmonic potentials

Another way to test the robustness of our findings is by modification of the trapping potential, keeping its equidistant spectral structure. Some special 1D potentials which maintain this property can be found in Ref. [99]:

$$V^{(1)}(x) = \frac{x^2}{2} + \frac{s^2 - 1}{8x^2}, \quad (30)$$

$$V^{(2)}(x) = \frac{x^2}{2} + \frac{3}{x^2} + \frac{4x^4 + 3}{(2x^2 + 3)^2} + \frac{4}{3}, \quad (31)$$

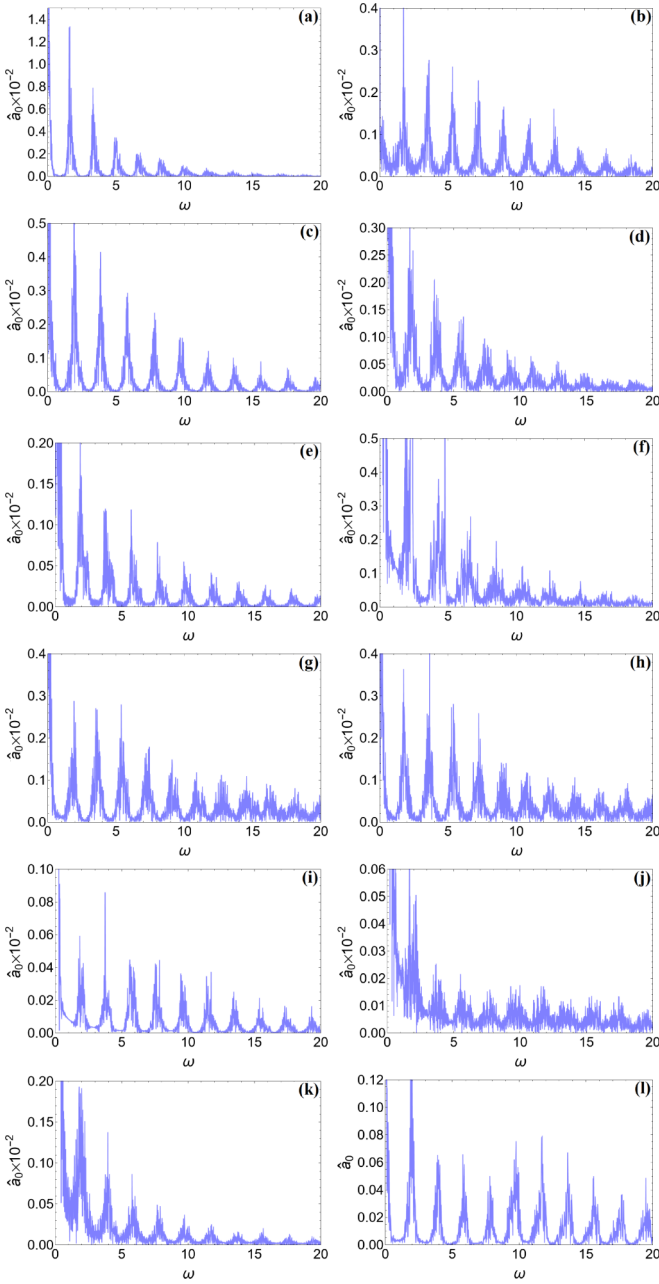


FIG. 6. Comblike power spectra produced by the 1D, 2D, and 3D GPEs (a)–(c), by the 1D, 2D, and 3D quintic NLSEs with the HO potential (d)–(f), by the 1D NLSE with potentials  $V^{(1)}$ ,  $V^{(2)}$ ,  $V^{(3)}$ ,  $V^{(4)}$  defined by Eqs. (30)–(33) [panels (g)–(j), respectively], by the two-component NLSE (37) (k), and by the relativistic real wave equation (38) (l).

$$V^{(3)}(x) = \frac{x^2}{2} + \frac{8x^2 - 4}{(2x^2 + 1)^2} + \frac{2}{3}, \quad (32)$$

$$V^{(4)}(x) = \frac{x^2}{2} + 8 \frac{(8x^6 + 12x^4 + 18x^2 - 9)}{(4x^4 + 12x^2 + 3)^2} + 2, \quad (33)$$

where  $s > 1$  is a constant,  $x \in (0, \infty)$  for the first two potentials, and  $x \in (-\infty, \infty)$  for the last two. In particular, potential  $V^{(1)}(x)$  in Eq. (30) represents the so-called “superselection”, *viz.*, the interaction of a particle, confined by

the HO potential and carrying a permanent dipole electric moment, with an electric charge placed at  $x = 0$  [100], while  $V^{(2)}(x)$  is a modified version of the same potential, in the case when the quasi-1D (cigar-shaped) trap is embedded in a partly screening host medium. Moreover, the 1D GPE with potential  $V^{(1)}(x)$  is identical to the radial reduction of the D-dimensional NLSE with the HO potential and nonlinear term  $r^{D-1}|\psi|^2\psi$  (see Appendix D for the derivation). In any case, this equation is truly different from Eqs. (2) and (29), constituting a new element for our study of HRP. Potentials  $V^{(3)}(x)$  and  $V^{(4)}(x)$  do not have a straightforward physical interpretation, but they provide additional relevant realizations of equidistant spectra.

The energy eigenvalues are fully equidistant for  $V^{(1)}$  and  $V^{(2)}$ ,

$$E_n^{(1)} = 2n + 1 + \frac{s}{2}, \quad E_n^{(2)} = 2n + \frac{23}{6}, \quad (34)$$

with  $n \geq 0$ . However, for  $V^{(3)}$  and  $V^{(4)}$  there is a gap between the ground-state eigenvalue and ones corresponding to the excited states, which form equidistant arrays (“towers”):

$$E_0^{(3)} = -\frac{5}{6}, \quad E_{n \geq 1}^{(3)} = n + \frac{7}{6}, \quad (35)$$

$$E_0^{(4)} = -\frac{3}{2}, \quad E_{n \geq 1}^{(4)} = n + \frac{5}{2}. \quad (36)$$

#### D. A two-component NLSE system

Another possibility [58,101–104] to realize the comblike (nonergodic) power spectra is offered by a two-component 1D NLSE,

$$\begin{aligned} i\partial_t u &= -\frac{1}{2}\partial_{xx}u + \frac{x^2}{2}u + cv + g_u|u|^2u, \\ i\partial_t v &= -\frac{1}{2}\partial_{xx}v + \frac{x^2}{2}v + cu + g_v|v|^2v, \end{aligned} \quad (37)$$

where  $g_u$ ,  $g_v$ , and  $c$  are constants. The linear version of the system decouples into two single-component equations for  $\psi_+ = u + v$  and  $\psi_- = u - v$ , which gives rise to two “towers” of equidistant energy eigenvalues,  $E_n^{(\pm)} = n + \frac{1}{2} \pm c$ .

#### E. A wave equation in anti-de Sitter spacetime

Our considerations of the comblike spectra are based on the equidistant energy spectrum (1), and depend little on peculiarities of the NLSEs. We have further tested the validity of the principles formulated here for the case of a relativistic wave equation whose normal-mode frequencies also fit condition (1). This choice is motivated by the connection between the GPE and the following equation for a real scalar field  $\phi$  in the anti-de Sitter spacetime [95,98,105]:

$$\partial_{tt}\phi = \cot^2 x \partial_x(\tan^2 x \partial_x\phi) + g\phi^3, \quad (38)$$

which is subject to boundary condition  $\phi(t, \pi/2) = 0$ , where  $x \in [0, \pi/2)$  is the radial coordinate. This equation gives rise to an equidistant spectrum,  $E_n = 2n + 3$ .

## VI. DISCUSSION

Our analysis has revealed that NLSEs with HRP (highly resonant potentials) pose a barrier to the emergence of

ergodic power spectra in weakly and strongly nonlinear regimes alike. While usually the consideration of nonergodic dynamics is restricted to small deformations of integrable equations [8–12,15–18,22–24], our focus has been on mechanisms that do not directly rely on proximity to integrability. The potentials in question, namely, the ones with equidistant linear spectra of energy eigenvalues [in particular, the HO (harmonic-oscillator) potential], produce a strong impact on the power spectra of the full nonlinear system, which remain concentrated in comblike arrays of spikes. This pattern is captured by our analytical consideration for weak nonlinearity, performed in Sec. III, and numerical simulations of the strongly nonlinear regime in Sec. IV. These spectra are in clear contrast with the continuous ones produced by generic potentials, and resemble quasidiscrete spectra associated with integrable dynamics.

While the difference between the HRP and generic potentials without any resonances is obvious, the difference is more subtle when comparing HRP to potentials that feature some resonances in their spectra, but the energy levels do not fit the rigid pattern defined by Eq. (1). In the case of generic potentials, normal-mode frequencies are incommensurate, and combinational frequencies created by nonlinearities quickly populate the real line, creating a generic continuum power spectrum. For that reason, much of our study has been focused on the peculiar but physically motivated case of the infinitely deep box potential. In that case, the linear normal-mode frequencies and all of their combinations are integers, which, however, does not preclude the emergence of the continuum power spectrum at a finite nonlinearity strength, in contrast to what is seen in the case of the HO and other HRPs with linear energy spectra in the form of Eq. (1). The analytical consideration carried out in Sec. III, together with numerical experiments reported in Secs. IV and V, make it clear that a central role is played by the spectrum of linear energy eigenvalues, even in the case of strong nonlinearity. We have seen, in the weakly nonlinear regime, how they determine the interactions between the modes in the system, which translates into the structure of the power spectrum. Equidistant energy eigenvalues, like those in the case of the HO potential, distribute the interactions in such a special way that a reduced set of frequencies dominate in the power spectrum, providing strong suppression of high frequencies and ensuring the protection of the nonergodic comblike power spectra in the regime of stronger nonlinearity. However, the quadratic energy eigenvalues produced by the box-shaped potential do not provide for the suppression of higher frequencies, and give rise to truly continuous ergodic spectra. This analysis is extended to a broad class of HRPs in Appendix B, leading to the same conclusion. Further, we have made use of simulations to study the dependence of the comblike power spectrum on the nonlinearity strength, and tested the genericity of our conclusions, checking them for NLSEs with various HRPs. Random waves were used as initial conditions to capture the evolution of a wide range of inputs. Our numerical results corroborate that the analysis developed in the weak-nonlinearity limit correctly forecasts the qualitative shape of the power spectra in the strongly nonlinear regime as well. We also inspected the distinction between the cases of focusing and defocusing nonlinearities,

concluding that the comblike power spectra degrade faster with the growth of the nonlinearity strength in the former case.

In general, linear features tend to get rapidly overwhelmed by nonlinear effects when the system departs from the weakly nonlinear regime, although some models for 1D random waves demonstrate regimes where dynamical features of weak and strong nonlinearities coexist [106] (i.e., random waves and coherent modes, such as solitons, exist in both regimes). HRPs admit similar coexistence between the features of weak and strong nonlinearity: while solitons (and other essentially nonlinear modes) are involved in the dynamics, it is still heavily influenced by the weak-nonlinearity features, such as the structure of the spectrum of energy eigenvalues. As a result, the comblike power spectra, which are directly associated with weakly nonlinear dynamics, persist for stronger nonlinearity.

After producing the basic results with the help of the guiding example of the 1D GPE with the HO potential, we have demonstrated that the same mechanism of the obstruction to ergodicity is maintained by generic HRPs. To do that, in addition to the analytical description developed in Sec. III and Appendix B, we have explored several NLSEs with this class of potentials. We observed comblike power spectra in the presence of different nonlinear terms, different potentials (belonging to the HRP class), different spatial dimensions, and in the two-component GPE as well. The presence of the multidimensional models in the class of highly resonant NLSEs, such as the 2D and 3D GPEs, and the quintic NLSE with the HO potential, are noteworthy findings. This is in contrast to studies of nonergodic dynamics that rely on proximity to integrability, as a vast majority of integrable equations are one-dimensional. In this work, we have studied the obstruction to ergodicity in the multidimensional equations under the assumption of the spherical symmetry. It would be interesting to lift this condition, addressing fully multidimensional spectra for states carrying angular momentum.

The presence of the 2D-GPE with the HO in the class of HRPs suggests a potential connection between our results and experiments on wave thermalization in multimode optical fibers, a topic of many ongoing experiments [86–90,107,108]. Light propagation in graded-index multimode fibers, studied in these experiments, is modeled by the finite-mode version of the 2D-GPE with the HO potential [86–90]. In this setup, Refs. [87,90] have studied the role played by structural disorder (addition of a random term to the HO) on the dynamics of weakly interacting random waves. Rapid thermalization has been observed in the presence of disorder, while the thermalize was hindered in the absence of this element (i.e., in the case of the pure HO potential). The thermalization is commonly explained in terms of the wave-turbulence theory, and no hindrances were expected when the experiments started. It is plausible that the anomaly pointed out in Refs. [87,90] may be caused by the influence of the equidistant energy eigenvalues inherent to the model that governs the observed dynamics, agreeing in this way with our inference that the specific structure of eigenvalues (in this case, produced by the 2D NLSE with the HO potential) may account for deviations from the ordinary principles of nonequilibrium dynamics. It would be interesting to investigate whether the

phenomenology of the effective nonergodicity observed in Refs. [87,90] is generic for other models with HRPs.

Finally, our study suggests an extension of the concept of quasi-integrability, identified in the form of quasisdiscrete power spectra in the 1D GPE with the HO potential and self-defocusing cubic nonlinearity in Ref. [49]. In that context, the case of self-focusing remained unexplored till now. We have tackled it here too, demonstrating the presence of the comblike power spectra in this case as well, although they degrade faster with the growth of the nonlinearity strength. We have provided an analytical description of this effect in the regime of weak nonlinearity, while previously reported results were purely numerical. Finally, we have broadened the understanding of the quasi-integrability by showing that its characteristic quasisdiscrete power spectrum, produced by the evolution of random-wave initial conditions, is shared by a large class of the nonlinear models including HRPs. Thus, our results imply that the 1D GPE with the HO potential is not exceptional in this regard, although it is worthwhile to mention the large range of values of the strength of the defocusing nonlinearity for which this physically relevant model produces well-defined comblike power spectra. While we have mostly focused on NLSEs, our weakly nonlinear analytics suggests that the obstruction-to-ergodicity mechanism should be present in equations of other types, such as nonlinear wave equations. We have briefly demonstrated the latter possibility by presenting the comblike power spectrum generated by the highly resonant real wave equation (38).

**ACKNOWLEDGMENTS**

A.B. thanks A. Picozzi, Z. Hani, G. Staffilani, and J. Amette for useful discussions. In the course of this work A.B. has been supported by the Polish National Science Centre Grant No. 2017/26/A/ST2/00530 and by the LabEx ENS-ICFP: ANR-10-LABX-0010/ANR-10-IDEX-0001-02 PSL\*. O.E. has been supported by Thailand NSRF via PMU-B (Grants No. B01F650006 and No. B05F650021) and by FWO-Vlaanderen through Project No. G006918N. B.A.M. has been supported, in part, by the Israel Science Foundation (Grant No. 1695/22).

**APPENDIX A: NUMERICAL METHODS**

Numerical simulations of NLSEs have been performed using two schemes. One is based on a pseudo-spectral decomposition of the spatial coordinate similar to that used in Refs. [80,83,109] and the fourth-order Runge-Kutta (4RK) method to advance in time. When the spatial coordinate is unbounded,  $x \in (-\infty, \infty)$ , such as in the case of the 1D GPE with the HO potential, we truncate the domain to a finite one  $x \in [-R_{\max}, R_{\max}]$  with  $R_{\max}$  large enough to guarantee that  $|\psi(t, \pm R_{\max})|$  is exponentially suppressed. This interval is discretized into  $N$  points of the form  $x_n = R_{\max}(\frac{2n}{N} - 1)$  with  $n = 0, 1, \dots, N - 1$ . The goal of this procedure is to compute the second derivative on the RHS of the equation by using the Fast Fourier transform (FFT), see Ref. [110] for a deep description. For this purpose, we decompose function  $\psi(t_j, x_n)$  at time  $t_j$  over the truncated set of the lowest  $N/2$

Fourier modes propagating to the left and to the right,

$$\psi(t_j, x_n) \approx \sum_{k=0}^{N/2-1} \beta_k^{(-)} e^{-i\frac{\pi}{R_{\max}}k(x_n+R_{\max})} \tag{A1}$$

$$+ \sum_{k=1}^{N/2} \beta_k^{(+)} e^{i\frac{\pi}{R_{\max}}k(x_n+R_{\max})}, \tag{A2}$$

where  $\beta_k^{(\pm)}$  are the Fourier amplitudes at time  $t_j$ . We apply the FFT to  $\psi(t_j, x_n)$  to compute the amplitudes, and use the inverse FFT to compute the second derivative,

$$\partial_{xx}\psi(t_j, x_n) \approx \sum_{k=1}^{N/2-1} -\left(\frac{\pi}{R_{\max}}k\right)^2 \beta_k^{(-)} e^{-i\frac{\pi}{R_{\max}}k(x_n+R_{\max})} \tag{A3}$$

$$+ \sum_{k=1}^{N/2} -\left(\frac{\pi}{R_{\max}}k\right)^2 \beta_k^{(+)} e^{i\frac{\pi}{R_{\max}}k(x_n+R_{\max})}. \tag{A4}$$

Note that the boundary conditions  $|\psi(t_j, \pm R_{\max})| \ll 1$  require that  $\beta_0^{(-)} \approx 0$  and  $\beta_k^{(+)} \approx -\beta_k^{(-)}$ . We use these conditions as a quality check in our simulations. Terms on the RHS of the equation that do not involve differentiation are computed using  $\psi(t_j, x_n)$ .

Our second scheme to simulate NLSEs is similar to that employed in Refs. [49,98]. It truncates the spatial domain to  $x \in [-R_{\max}, R_{\max}]$  as well, and discretizes it to  $x_n = R_{\max}(\frac{2n}{N} - 1)$  with  $n = 0, 1, \dots, N$ . We use, in this case, the finite-difference method to compute spatial derivatives like in Refs. [49,98], while the 6RK algorithm is used to advance in time. The two schemes have shown an excellent agreement, conserving the norm  $M$  (3) and energy  $H$  (4), with maximum deviations at the level of the numerical precision  $\sim 10^{-13}$  for the first scheme, and  $\sim 10^{-13}$  for  $M$ ,  $\sim 10^{-8}$  for  $H$  in the second scheme in the HO, while  $\sim 10^{-9}$  for  $M$ ,  $\sim 10^{-5}$  for  $H$  in the box. The codes have been implemented in C++, running parallel computations on a GPU to speed up the simulation. The number of points that we used varies depending on the initial data and the setup—typically,  $N$  ranges from  $2^{13}$  to  $2^{17}$  in the case of the HO potential, and from  $2^{11}$  to  $2^{13}$  in the case of the box potential. It is relevant to mention that the same results can be produced by dint of the split-step integration method implemented in the usual numerical shell, cf. Ref. [111].

**APPENDIX B: THE DECAY OF  $\mathcal{S}_n(k)$**

We show here that amplitudes

$$\mathcal{S}_n(k) \equiv \underbrace{\sum_{m=0}^{\infty} \sum_{i=0}^{\infty} \sum_{j=0}^{\infty} C_{nmi} \bar{\alpha}_m \alpha_i \alpha_j}_{\Delta_{nmi} = \mathcal{V}_k} \tag{B1}$$

are strongly suppressed at large  $|n - k|$  in highly resonant systems, with spectra

$$E_n = an + b \quad \text{with } n \in \mathbb{N}, a, b \in \mathbb{R}, \tag{B2}$$

for configurations of  $\alpha_n$  that actually occur in the course of the evolution (with an exponential suppression at large  $n$ ). First, Fig. 7 visually illustrates the fact that the suppression

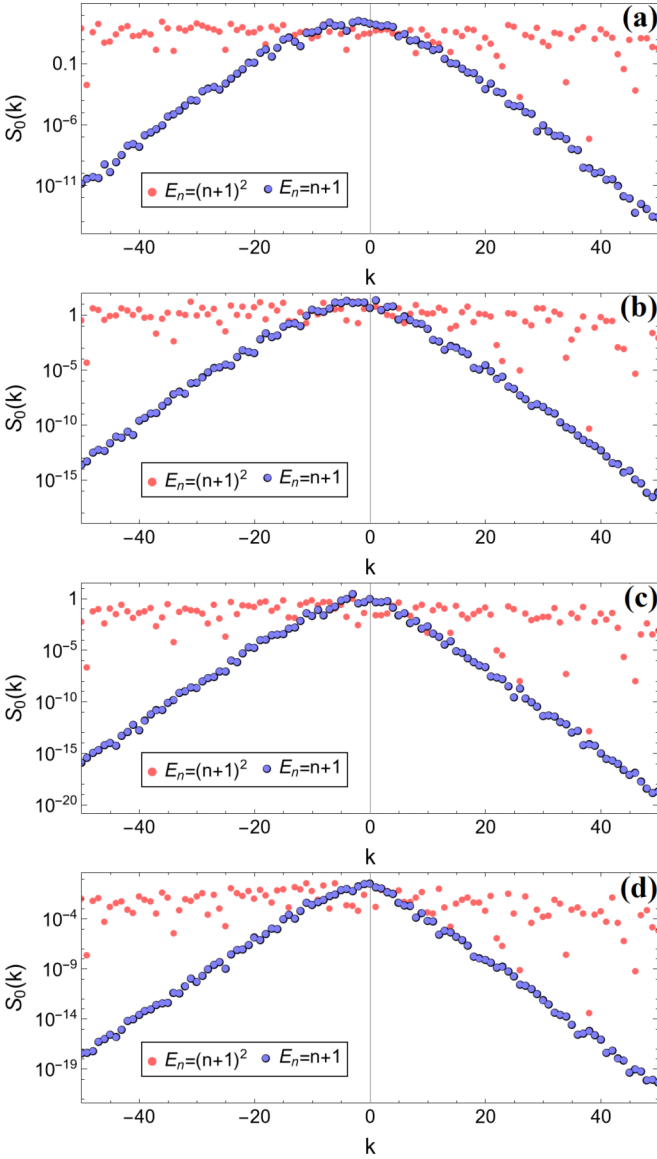


FIG. 7. Comparison between amplitudes  $\mathcal{S}_0(k)$  for the linear  $E_n = n + 1$  and quadratic  $E_n = (n + 1)^2$  spectra of the energy eigenvalues. In each plot, we have used the same values of  $\alpha_n$  and  $C_{nmij}$  for both sets of eigenvalues, as per Eqs. (B4) and (B5). The difference between the plots is the power of  $C_{nmij}$ ,  $r = 3, 1.5, 0, -1$ , from top to bottom.

of  $\mathcal{S}_n(k)$  at large  $|n - k|$  depends very little on the couplings  $C_{nmij}$ , irrespective of the decay or growth with the variation of the indices, but, in contrast, it strongly depends on the equidistant relation of eigenvalues (B2). In each plots of Fig. 7 we have numerically calculated the values of  $\mathcal{S}_n(k)$ , using the same set of  $C_{nmij}$  and  $\alpha_n$  but two different choices of eigenvalues, equidistant  $E_n = n + 1$  and quadratic  $E_n = (n + 1)^2$  ones. This may seem as a minor difference because  $E_n$  only affects the computation of expression (B1) through

$$\Delta_{nmij} = E_n + E_m - E_i - E_j, \quad (\text{B3})$$

to restrict the interactions to frequency  $\mathcal{W}_k$ . However, it leads to a dramatic difference between the behavior of  $\mathcal{S}_n(k)$  at moderate and large values of  $|n - k|$  for the equidistant and

quadratic energy eigenvalues. As we observe in all plots of Fig. 7, in the equidistant case these amplitudes rapidly decay with the increase of  $|n - k|$  (resembling an exponential decay), while this does not happen in the quadratic case. For those specific plots we have used

$$\alpha_n = (n + 1)^2 e^{-n} \mathcal{A}_n e^{i\mathcal{P}_n}, \quad (\text{B4})$$

$$C_{nmij} = (n + m + i + j + 1)^r, \quad (\text{B5})$$

where  $\mathcal{A}_n$ , and  $\mathcal{P}_n$  are random variables uniformly distributed on  $[0, 1]$  and  $[0, 2\pi)$ , respectively, while power  $r$  gave the opportunity to find out if the coefficients decay ( $r < 0$ ), remain constant ( $r = 0$ ), or grow ( $r > 0$ ) with the variation of the indices. Note that expression (B4) captures the qualitative behavior of  $\alpha_n$  in our numerical simulation, as explained in Sec. III. Other choices from this class of conditions lead to the same conclusion. For  $C_{nmij}$  we have used the power law in Eq. (B5) because they exhibit, at most, a polynomial growth with the increase of the indices in all physically relevant systems we are aware of. For instance, the  $D$ -dimensional GPE with the HO potential has asymptotic values  $C_{nmnm} \sim n^{\frac{D}{2}-2}$  for large  $n$  [98], and similar asymptotics have been found for relativistic wave equations [112–114]. Other choices of  $C_{nmij}$  in this class lead to the same conclusion as well.

Next, we aim to show that the exponential decay of  $\mathcal{S}_n(k)$  for the highly resonant systems (B2) may be derived analytically, arriving at the result

$$|\mathcal{S}_n(k)| < e^{-\beta|n-k|} P_{n,k}, \quad (\text{B6})$$

with  $\beta > 0$ , where  $P_{n,k}$  is a polynomial in  $n$  and  $k$  that depends on the detailed form of  $\alpha_n$  and  $C_{nmij}$ . To derive this bound, we use an estimate for the exponential decay of  $\alpha_n$  at large  $n$ , which is what actually happens in our simulations, and an arbitrary polynomial  $p_n^{(s)}$  in  $n$  of degree  $s > 0$  to bound different values of  $\alpha_n$ . Thus, this estimate takes the form of  $|\alpha_n| < p_n^{(s)} e^{-\beta n}$  where  $\beta > 0$  is not specified and appears in Eq. (B6), as we show below. For the couplings, we are going to use an estimate based on an arbitrary polynomial  $q_n^{(r)}$  in  $n$  of degree  $r > 0$  for each index,  $|C_{nmij}| < Q_{nmij}^{(r)} \equiv q_n^{(r)} q_m^{(r)} q_i^{(r)} q_j^{(r)}$ . This estimate comes from the observation that the couplings have a polynomial growth at most for large values of the indices, as mentioned above. An estimate admitting each index to have a different power may be used, but it can be covered by the present choice, simply setting  $r$  equal to the largest power. Plugging the estimates for  $\alpha_n$  and  $C_{nmij}$  into the expressions for  $\mathcal{S}_n(k)$  (B1), we obtain

$$\begin{aligned} |\mathcal{S}_n(k)| &= \left| \sum_{m=0}^{\infty} \sum_{i=0}^{\infty} \sum_{j=0}^{\infty} C_{nmij} \bar{\alpha}_m \alpha_i \alpha_j \right| \\ &\quad \underbrace{\hspace{10em}}_{n+m-i-j=k} \\ &< \sum_{m=0}^{\infty} \sum_{i=0}^{\infty} \sum_{j=0}^{\infty} |C_{nmij}| |\bar{\alpha}_m| |\alpha_i| |\alpha_j| \\ &\quad \underbrace{\hspace{10em}}_{n+m-i-j=k} \\ &< \sum_{m=0}^{\infty} \sum_{i=0}^{\infty} \sum_{j=0}^{\infty} Q_{nmij}^{(r)} p_m^{(s)} p_i^{(s)} p_j^{(s)} e^{-\beta(m+i+j)}. \quad (\text{B7}) \\ &\quad \underbrace{\hspace{10em}}_{n+m-i-j=k} \end{aligned}$$

The constraint on the indices,  $n + m - i - j = k$ , may be used to remove the summation in  $j$ . Two cases must be distinguished, *viz.*,  $k < n$  and  $k \geq n$ , to guarantee that  $j \geq 0$ .

*Case  $k < n$ :* Substituting  $j = n + m - k - i$  one gets

$$|\mathcal{S}_n(k)| < e^{\beta(k-n)} \sum_{m=0}^{\infty} e^{-2\beta m} p_m^{(s)} \times \sum_{i=0}^{n-k+m} \mathcal{Q}_{nmi(n-k+m-i)}^{(r)} p_i^{(s)} p_{(n-k+m-i)}^{(s)}. \quad (\text{B8})$$

We know that the sum  $\sum_{i=1}^M i^a$  with  $a \geq 0$  is a polynomial of degree  $a + 1$  in  $M$  [115]. Then, the estimate in index  $i$  is a polynomial  $n, m$ , and  $k$ , denoted by  $F_{n,m,k}$ . We use now that  $\sum_{m=0}^{\infty} e^{-2\beta m} (m+1)^b$  with  $b \in \mathbb{R}$  and  $\beta > 0$  is a finite number to get

$$|\mathcal{S}_n(k)| < e^{\beta(k-n)} \sum_{m=0}^{\infty} e^{-2\beta m} p_m^{(s)} F_{n,m,k} < P_{n,k} e^{\beta(k-n)}, \quad (\text{B9})$$

where  $P_{n,k}$  is a polynomial in  $n$  and  $k$  respectively.

*Case  $k \geq n$ :* In this case one has to be careful with the ranges of  $m$  and  $i$  to guarantee that  $j \geq 0$ . Taking this into account, the expression for  $\mathcal{S}_n(k)$  is

$$|\mathcal{S}_n(k)| < e^{\beta(k-n)} \sum_{m=k-n}^{\infty} e^{-2\beta m} p_m^{(s)} \times \sum_{i=0}^{n-k+m} \mathcal{Q}_{nmi(n-k+m-i)}^{(r)} p_i^{(s)} p_{(n-k+m-i)}^{(s)} = e^{\beta N} \sum_{M=0}^{\infty} e^{-2\beta M} p_{M+N}^{(s)} \sum_{i=0}^M \mathcal{Q}_{n(M+N)i(M-i)}^{(r)} p_i^{(s)} p_{(M-i)}^{(s)}, \quad (\text{B10})$$

where we have made the following changes,  $N = n - k$  and  $M = m + N$ , to remove the dependence of the lowest value of  $m$  on  $k - n$ . Note that these changes flipped the sign in the first exponential. The resulting expression is similar to the one for the case of  $k < n$ , and we proceed using the same properties to conclude that

$$|\mathcal{S}_n(k)| < e^{\beta(n-k)} P_{n,k}, \quad (\text{B11})$$

where in this case  $P_{n,k}$  is a polynomial in  $n$  and  $k$ . The combination of Eqs. (B9) for  $k < n$  and (B11) for  $k \geq n$  results in Eq. (B6).

One may also derive an estimate similar to Eq. (B1) for case of the box potential, but the quadratic eigenvalues (9) make this process a bit more involved than in the case of the equidistant eigenvalues. The difficulties appear in the constraint imposed on the indices (B3),

$$k = (n+1)^2 + (m+1)^2 - (i+1)^2 - (j+1)^2. \quad (\text{B12})$$

Using the above-mentioned estimates  $|\alpha_n| < p_n^{(s)} e^{-\beta n}$ , and  $|C_{nmij}| < q_n^{(r)} q_k^{(r)} q_i^{(r)} q_j^{(r)}$  one may see that

$$|\mathcal{S}_n(k)| < D_{n,k} e^{-\beta \sqrt{|k-(n+1)^2|}}, \quad (\text{B13})$$

where  $D_{n,k}$  is a polynomial in  $n$  and  $k$ , and  $\beta$  is again the exponent of  $|\alpha_n|$ . Note that in this case the suppression of

frequencies is much weaker than for the equidistant energy spectrum. This estimate comes from assessing the dominant contribution of  $N \equiv k - (n+1)^2$  in  $|\mathcal{S}_n(k)|$  according to Eq. (B1),

$$|C_{nmij}| |\bar{\alpha}_m| |\alpha_i| |\alpha_j| < \mathcal{Q}_{nmij}^{(r)} p_m^{(s)} p_i^{(s)} p_j^{(s)} e^{-\beta(m+i+j)}. \quad (\text{B14})$$

The key part of this expression is the  $\exp[-\beta(m+i+j)]$ , which must be studied in two parts. *Case  $N \geq 0$ :* We use the relation (B12) between the indices, to obtain

$$m = \sqrt{k - (n+1)^2 + (i+1)^2 + (j+1)^2} - 1. \quad (\text{B15})$$

Plugging this expression in the exponent one arrives to the following expression:

$$-\beta(m+i+j) = -\beta(\sqrt{N + (i+1)^2 + (j+1)^2} - 1) - \beta(i+j). \quad (\text{B16})$$

As  $i, j \geq 0$ , the first term is directly bounded by  $-\beta\sqrt{N}$ , getting

$$\sum_{i=0}^{\infty} \sum_{j=0}^{\infty} \mathcal{Q}_{nmij}^{(r)} p_m^{(s)} p_i^{(s)} p_j^{(s)} e^{-\beta(m+i+j)} \leq e^{-\beta\sqrt{N}} \sum_{i=0}^{\infty} \sum_{j=0}^{\infty} \mathcal{Q}_{nmij}^{(r)} p_m^{(s)} p_i^{(s)} p_j^{(s)} c e^{-\beta(i+j)} \leq D_{n,k} e^{-\beta\sqrt{N}}, \quad (\text{B17})$$

where  $D_{n,k}$  is a polynomial in  $n, k$ , and we have used the following properties to reach the last expression. First, we used constant  $c$  large enough to bound the independent term in the exponent. We also used the fact that  $\sum_{i=0}^{\infty} e^{-\beta i} (i+1)^b$  with  $b \in \mathbb{R}$  and  $\beta > 0$  takes a finite value to bound the sums in the intermediate expression independently of the upper limit. Finally, we used a polynomial  $D_{n,k}$  of high enough degree to bound the terms involving  $n$  and  $k$ .

*Case  $N < 0$ :* We use  $j$  instead of  $m$  in this case,

$$j = \sqrt{-N + (m+1)^2 - (i+1)^2} - 1. \quad (\text{B18})$$

We define  $I = i + 1$  and  $M = (m+1)^2 - N$  to write the exponent in the following form:

$$-\beta(m+i+j) = -\beta(\sqrt{M - I^2} + I) + 2\beta - \beta m. \quad (\text{B19})$$

To guarantee that  $j \geq 0$  index  $I$  take the integer values in  $[1, \sqrt{M-1}]$ . Because of the symmetry  $i \leftrightarrow j$  we just need to consider the values of  $I$  in  $[1, \sqrt{M}/2]$ , namely,  $i$  from 0 to  $j$ . In this interval, we are going to obtain an upper bound for the first term on the RHS of Eq. (B19). Adding and subtracting  $\beta\sqrt{M}$  yields

$$-\beta(\sqrt{M - I^2} + I) = -\beta\sqrt{M} + \beta(\sqrt{M} - I - \sqrt{M - I^2}) \leq -\beta\sqrt{M} - (2 - \sqrt{2})I. \quad (\text{B20})$$

The later inequality is obtained by showing that the first derivative of the LHS is negative in  $[0, \sqrt{M}/2]$ , the second derivative is positive in the same interval, and the RHS and LHS coincide at the edges of the interval. A final step is  $-\beta\sqrt{M} < -\beta\sqrt{|N|}$  because  $m \geq 0$ . From this point one repeats the same argument as before to bound the sums in  $m$

and  $i$  obtaining the estimate (B13) for  $|\mathcal{S}_n(k)|$  in the case of the box potential.

### APPENDIX C: POWER SPECTRUM FROM LONGER-TIME EVOLUTION

We demonstrate that the comblike structure of the power spectrum is present at times longer than those used in the main text. To do so, we have simulated the initial data presented in Fig. 2(I) for a total time of  $t_{\max} = 10^4$ , much larger than the time used before  $t_{\max} = 500$ . The results are presented in Fig. 8. No significant difference is appreciated with respect to Fig. 2 in the global shape of the profile and the evolution of the energies in this new scale. We also observe that the comblike structure of the power spectrum is present as illustrated by Fig. 8(c). For  $t_{\max} = 10^4$  the amplitude of the spectrum is smaller than for  $t_{\max} = 500$  (both spikes and valleys). This effect does not have impact on the comblike structure, it is just a matter of improvement in the resolution of frequencies ( $\Delta\omega = 2\pi/t_{\max}$ ) which allows to discern now ( $t_{\max} = 10^4$ ) slightly different frequencies interpreted as a single one before ( $t_{\max} = 500$ ). Note that both spikes and valleys in the power spectrum are affected by the same effect Fig. 8(d). Furthermore, one may observe in Fig. 8(e) the agreement between the power spectrum calculated from the first and the last 500 units of time (without adjustable parameters), indicating no change in the governing dynamics. Figure 9 also confirms the presence of the comblike power spectrum displayed by the quintic 1D-NLSE with the HO potential (28) at different timescales.

These results suggest the presence of the comblike power spectrum at times larger than  $t_{\max} \sim 10^4$ . Dynamics acting at very large timescales may be present, and in such a case, most of the effects on the power spectrum should be concentrated at small frequencies ( $\omega$  proportional to the inverse of the scale) or slowly get present as  $t_{\max}$  grows. For instance, it is expected that for generic wave systems the exponential suppression of high-modes  $\alpha_n$  is gradually replaced by a power-law at very long times [116–118]. In that case, the specific values of the couplings between modes  $C_{nmi}$  in Eq. (15) should play an important role in the preservation or erosion of any structure in the power spectrum.

### APPENDIX D: EIGENSTATES

We collect here results for the Schrödinger equations introduced in the main text. The results for the 1D Schrödinger equation with the HO and box potentials are provided above in Eqs. (8) and (9).

*Schrödinger equation (29) with the HO potential in D dimensions:*

$$E_n = 2n + \frac{D}{2}, \quad (\text{D1})$$

$$f_n(r) = \sqrt{\frac{n!\Gamma(D/2)}{\pi^{d/2}\Gamma(n+D/2)}} L_n^{(\frac{D-2}{2})}(r^2) e^{-r^2/2}, \quad (\text{D2})$$

where  $L_n^{(\alpha)}$  are the generalized Laguerre polynomials.

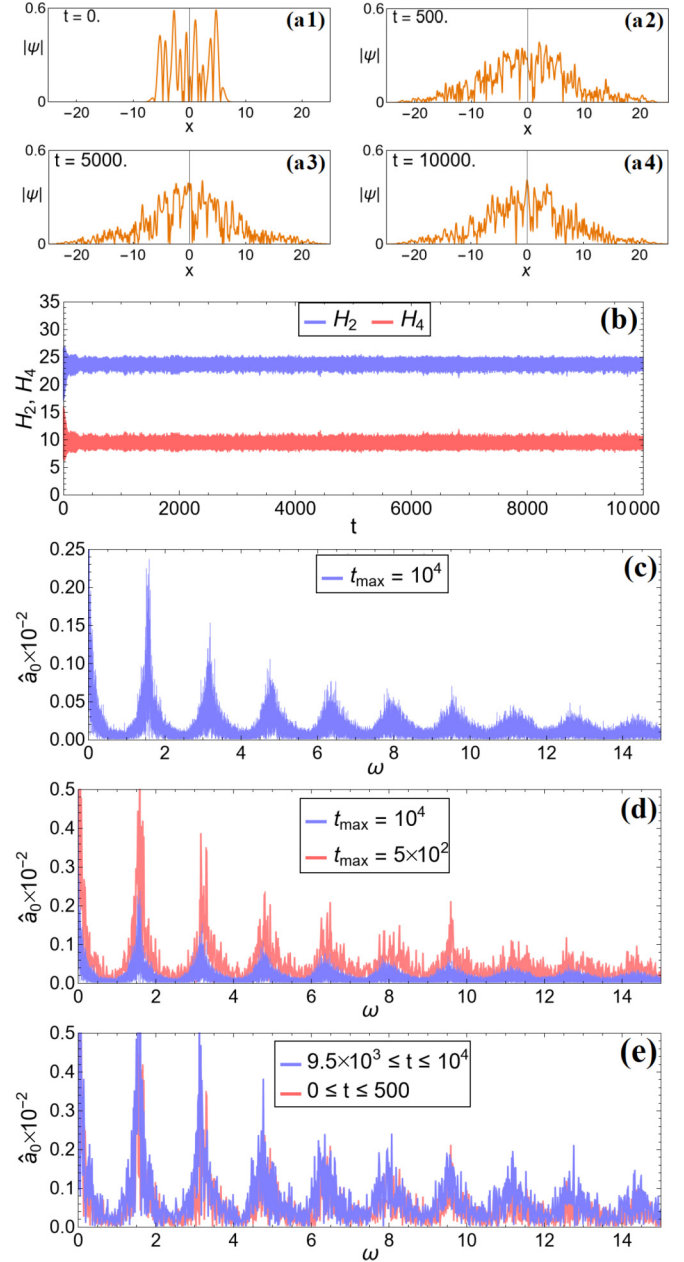


FIG. 8. Long-time evolution ( $t_{\max} = 10^4$ ) of the initial data shown in Fig. 2(I). From top to bottom: four snap-shots illustrating the shape of the profile in the course of the evolution (a); temporal evolution of the quadratic (5) and quartic (6) energies (b); power spectrum of the lowest-mode's amplitude calculated in the window of time  $[0, 10^4]$  (c); comparison of the power spectra calculated in the windows of time  $[0, 500]$  and  $[0, 10^4]$  (d); comparison of the power spectra calculated in the windows of time  $[0, 500]$  and  $[9500, 10^4]$  (e).

*1D Schrödinger equation with the “superselection” potential  $V^{(1)}(x)$  (30):*

$$E_n = 2n + \frac{\delta}{2}, \quad (\text{D3})$$

$$f_n(x) = \sqrt{\frac{n!\Gamma(\delta/2)}{\pi^{\delta/2}\Gamma(n+\delta/2)}} L_n^{(\frac{\delta-2}{2})}(x^2) e^{-x^2/2}, \quad (\text{D4})$$

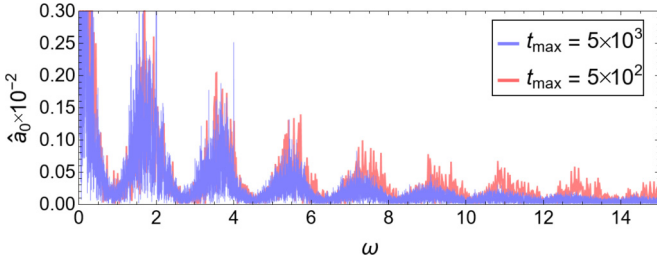


FIG. 9. Comparison between the power spectra of the lowest-mode's amplitude calculated in the window of time  $[0, 500]$  [the one shown in Fig. 6(d)] and a larger window  $[0, 5000]$  displayed by the quintic 1D NLSE with the HO potential (28).

where  $\delta = 2 + \sqrt{1 + 4s}$  and  $L_n^{(\alpha)}(x)$  are the generalized Laguerre polynomials.

We also show here how to derive the 1D-GPE with potential  $V^{(1)}$ , Eq. (30), from the dimensional reduction of the following D-dimensional NLSE with the HO potential:

$$i\partial_t \psi = \frac{1}{2} \left( -\partial_{rr} - \frac{D-1}{r} \partial_r + r^2 \right) \psi + gr^{D-1} |\psi|^2 \psi, \quad (\text{D5})$$

with  $r \in [0, \infty)$ , and the nonlinear term has the factor  $r^{D-1}$ . First, one has to plug the change  $\psi(t, x) = r^{\frac{1-D}{2}} \tilde{\psi}(t, r)$  into the equation to get rid of the first derivative in the radial Laplacian. Then, one cancels factor  $r^{\frac{1-D}{2}}$  on the RHS and LHS to get

$$i\partial_t \tilde{\psi} = -\frac{1}{2} \partial_{rr} \tilde{\psi} + \left( \frac{r^2}{2} + \frac{D^2 - 4D + 3}{8r^2} \right) \tilde{\psi} + g |\tilde{\psi}|^2 \tilde{\psi}, \quad (\text{D6})$$

which is the 1D-GPE with the anharmonic potential  $V^{(1)}$  (30) on the half-line.

*1D-Schrödinger equation with potential  $V^{(2)}(x)$  (31):*

$$E_n = 2n + \frac{23}{6}, \quad (\text{D7})$$

$$f_n(x) = \frac{2^{n+1/2} n!}{\pi^{1/4} \sqrt{(2n+5)(2n+1)(2n)!}} e^{-x^2/2} \quad (\text{D8})$$

$$\times \left( \frac{3(1+2x^2)}{(3+2x^2)} L_n^{(\frac{1}{2})}(x^2) - 2(n+1) L_{n+1}^{(-\frac{1}{2})}(x^2) \right), \quad (\text{D9})$$

where  $L_n^{(\alpha)}(x)$  are the generalized Laguerre polynomials.

*1D-Schrödinger equation with potential  $V^{(3)}(x)$  (32):*

$$E_0 = -\frac{5}{6}, \quad E_{n \geq 1} = n + \frac{7}{6}, \quad (\text{D10})$$

$$f_0(x) = \frac{\sqrt{2}}{\pi^{\frac{1}{4}}} \frac{e^{-\frac{x^2}{2}}}{1+2x^2}, \quad (\text{D11})$$

$$f_{n \geq 1}(x) = \frac{1}{\pi^{1/4} \sqrt{2^n(n+2)(n-1)!}} e^{-x^2/2} \quad (\text{D12})$$

$$\times \left( \frac{4x}{(1+2x^2)} H_{n-1}(x) + H_n(x) \right), \quad (\text{D13})$$

where  $H_n(x)$  are the Hermite polynomials.

*1D-Schrödinger equation with potential  $V^{(4)}(x)$  (33):*

$$E_0 = -\frac{3}{2}, \quad E_{n \geq 1} = n + \frac{5}{2}, \quad (\text{D14})$$

$$f_0(x) = \frac{2\sqrt{6}}{\pi^{\frac{1}{4}}} \frac{e^{-\frac{x^2}{2}}}{3+12x^2+4x^4}, \quad (\text{D15})$$

$$f_{n \geq 1}(x) = \frac{1}{\pi^{1/4} \sqrt{2^n(n+4)(n-1)!}} e^{-\frac{x^2}{2}} \quad (\text{D16})$$

$$\times \left( \frac{8x(3+2x^2)}{(3+12x^2+4x^4)} H_{n-1}(x) + H_n(x) \right), \quad (\text{D17})$$

where  $H_n(x)$  are the Hermite polynomials.

*Two-component 1D Schrödinger equation (37):* Using transformation  $\psi_+ = u + v$  and  $\psi_- = u - v$ , the equation produces two “towers” of eigenvalues,

$$E_n^{(\pm)} = n + \frac{1}{2} \pm c, \quad (\text{D18})$$

and the same eigenfunctions as above:

$$f_n^{(\pm)}(x) = \frac{1}{\pi^{1/4} \sqrt{2^n n!}} H_n(x) e^{-\frac{x^2}{2}}. \quad (\text{D19})$$

*A wave equation in the anti-de Sitter space (38):*

$$E_n = 2n + 3, \quad (\text{D20})$$

$$f_n(x) = \frac{2\sqrt{n!(n+2)!}}{\Gamma(n+\frac{3}{2})} \cos^3(x), P^{(\frac{1}{2}, \frac{3}{2})}(\cos 2x), \quad (\text{D21})$$

where  $P^{(\frac{1}{2}, \frac{3}{2})}$  are Jacobi polynomials.

- [1] S. B. Kuksin, *Nearly Integrable Infinite-dimensional Hamiltonian Systems*, Lecture Notes in Mathematics (Springer, Berlin, 1993), Vol. 1556.
- [2] A. J. Lichtenberg and M. A. Leiberman, *Regular and Stochastic Motion* (Springer Science & Business Media, Cham, 1983), Vol. 38.
- [3] B. Paredes, A. Widera, V. Murg, O. Mandel, S. Fölling, I. Cirac, G. V. Shlyapnikov, T. W. Hansch, and I. Bloch, Tonks-Girardeau gas of ultracold atoms in an optical lattice, *Nature (London)* **429**, 277 (2004).

- [4] T. Kinoshita, T. Wenger, and D. S. Weiss, A quantum Newton's cradle, *Nature (London)* **440**, 900 (2006).
- [5] E. H. Lieb and W. Liniger, Exact analysis of an interacting Bose gas. I. The general solution and the ground state, *Phys. Rev.* **130**, 1605 (1963).
- [6] V. A. Yurovsky, B. A. Malomed, R. G. Hulet, and M. Olshanii, Dissociation of One-Dimensional Matter-Wave Breathers Due to Quantum Many-Body effects, *Phys. Rev. Lett.* **119**, 220401 (2017).

- [7] T. Langen, R. Geiger, and J. Schmiedmayer, Ultracold atoms out of equilibrium, *Annu. Rev. Condens. Matter Phys.* **6**, 201 (2015).
- [8] B. Bertini, M. Collura, J. De Nardis, and M. Fagotti, Transport in Out-of-Equilibrium XXZ Chains: Exact Profiles of Charges and Currents, *Phys. Rev. Lett.* **117**, 207201 (2016).
- [9] O. A. Castro-Alvaredo, B. Doyon, and T. Yoshimura, Emergent Hydrodynamics in Integrable Quantum Systems Out of Equilibrium, *Phys. Rev. X* **6**, 041065 (2016).
- [10] A. Bastianello, A. De Luca, and R. Vasseur, Hydrodynamics of weak integrability breaking, *J. Stat. Mech.: Theory Exp.* (2021) 114003.
- [11] I. Bouchoule and J. Dubail, Generalized hydrodynamics in the one-dimensional Bose gas: Theory and experiments, *J. Stat. Mech.: Theory Exp.* (2022) 014003.
- [12] A. Bastianello, A. De Luca, B. Doyon, and J. De Nardis, Thermalization of a Trapped One-Dimensional Bose Gas Via Diffusion, *Phys. Rev. Lett.* **125**, 240604 (2020).
- [13] F. Møller, C. Li, I. Mazets, H.-P. Stimming, T. Zhou, Z. Zhu, X. Chen, and J. Schmiedmayer, Extension of the Generalized Hydrodynamics to the Dimensional Crossover Regime, *Phys. Rev. Lett.* **126**, 090602 (2021).
- [14] N. Malvania, Y. Zhang, Y. Le, J. Dubail, M. Rigol, and D. S. Weiss, Generalized hydrodynamics in strongly interacting 1D Bose gases, *Science* **373**, 1129 (2021).
- [15] M. Gring, M. Kuhnert, T. Langen, T. Kitagawa, B. Rauer, M. Schreitl, I. Mazets, D. A. Smith, E. Demler, and J. Schmiedmayer, Relaxation and prethermalization in an isolated quantum system, *Science* **337**, 1318 (2012).
- [16] D. Adu Smith, M. Gring, T. Langen, M. Kuhnert, B. Rauer, R. Geiger, T. Kitagawa, I. Mazets, E. Demler, and J. Schmiedmayer, Prethermalization revealed by the relaxation dynamics of full distribution functions, *New J. Phys.* **15**, 075011 (2013).
- [17] T. Langen, S. Erne, R. Geiger, B. Rauer, T. Schweigler, M. Kuhnert, W. Rohringer, I. E. Mazets, T. Gasenzer, and J. Schmiedmayer, Experimental observation of a generalized Gibbs ensemble, *Science* **348**, 207 (2015).
- [18] Y. Tang, W. Kao, K. Y. Li, S. Seo, K. Mallayya, M. Rigol, S. Gopalakrishnan, and B. L. Lev, Thermalization near Integrability in a Dipolar Quantum Newton's Cradle, *Phys. Rev. X* **8**, 021030 (2018).
- [19] M. Rigol, V. Dunjko, V. Yurovsky, and M. Olshanii, Relaxation in a Completely Integrable Many-Body Quantum System: An *Ab Initio* Study of the Dynamics of the Highly Excited States of 1D Lattice Hard-Core Bosons, *Phys. Rev. Lett.* **98**, 050405 (2007).
- [20] L. Vidmar and M. Rigol, Generalized Gibbs ensemble in integrable lattice models, *J. Stat. Mech.: Theory Exp.* (2016) 064007.
- [21] B. Doyon, Thermalization and pseudolocality in extended quantum systems, *Commun. Math. Phys.* **351**, 155 (2017).
- [22] X. Cao, V. B. Bulchandani, and J. E. Moore, Incomplete Thermalization from Trap-Induced Integrability Breaking: Lessons from Classical Hard Rods, *Phys. Rev. Lett.* **120**, 164101 (2018).
- [23] A. Hutsalyuk and B. Pozsgay, Integrability breaking in the one-dimensional Bose gas: Atomic losses and energy loss, *Phys. Rev. E* **103**, 042121 (2021).
- [24] K. F. Thomas, M. J. Davis, and K. V. Kheruntsyan, Thermalization of a quantum Newton's cradle in a one-dimensional quasicondensate, *Phys. Rev. A* **103**, 023315 (2021).
- [25] U. Niederer, Maximal kinematic invariance group of harmonic oscillator, *Helv. Phys. Acta* **46**, 191 (1973).
- [26] A. V. Turbiner, One-dimensional quasiexactly solvable Schrödinger equations, *Phys. Rep.* **642**, 1 (2016).
- [27] P. Villain and M. Lewenstein, Fermi-Pasta-Ulam problem revisited with a Bose-Einstein condensate, *Phys. Rev. A* **62**, 043601 (2000).
- [28] H. S. Dumas, *The KAM Story: A Friendly Introduction to the Content, History, and Significance of Classical Kolmogorov–Arnold–Moser Theory* (World Scientific, Singapore, 2014).
- [29] E. P. Gross, Structure of a quantized vortex in boson systems, *Nuovo Cim.* **20**, 454 (1961).
- [30] L. P. Pitaevskii, Vortex lines in an imperfect Bose gas, *Soviet J. Exp. Theor. Phys.* **13**, 451 (1961).
- [31] L. Pitaevskii and S. Stringari, *Bose Einstein Condensation* (Oxford University Press, Oxford, UK, 2003).
- [32] C. J. Pethick and H. Smith, *Bose-Einstein Condensation in Dilute Gases* (Cambridge University Press, Cambridge, UK, 2001).
- [33] C. F. Barenghi and N. G. Parker, *A Primer on Quantum Fluids* (Springer, Berlin, 2017).
- [34] V. E. Zakharov and A. B. Shabat, Exact theory of two-dimensional self-focusing and one-dimensional self-modulation of waves in nonlinear media, *Zh. Eksp. Teor. Fiz.* **61**, 118 (1971).
- [35] V. E. Zakharov and S. V. Manakov, On the complete integrability of a nonlinear Schrödinger equation, *Theoret. Math. Phys.* **19**, 551 (1974).
- [36] Yu. S. Kivshar and B. A. Malomed, Dynamics of solitons in nearly integrable systems, *Rev. Mod. Phys.* **61**, 763 (1989).
- [37] I. Březinová, L. A. Collins, K. Ludwig, B. I. Schneider, and J. Burgdörfer, Wave chaos in the nonequilibrium dynamics of the Gross-Pitaevskii equation, *Phys. Rev. A* **83**, 043611 (2011).
- [38] I. Březinová, A. U. Lode, A. I. Streltsov, O. E. Alon, L. S. Cederbaum, and J. Burgdörfer, Wave chaos as signature for depletion of a Bose-Einstein condensate, *Phys. Rev. A* **86**, 013630 (2012).
- [39] S. Donsa, H. Hofstätter, O. Koch, J. Burgdörfer, and I. Březinová, Long-time expansion of a Bose-Einstein condensate: Observability of Anderson localization, *Phys. Rev. A* **96**, 043630 (2017).
- [40] L. Ermann, E. Vergini, and D. L. Shepelyansky, Dynamics and thermalization of a Bose-Einstein condensate in a Sinaï-oscillator trap, *Phys. Rev. A* **94**, 013618 (2016).
- [41] J. Ruostekoski, B. Kneer, W. P. Schleich, and G. Rempe, Interference of a Bose-Einstein condensate in a hard-wall trap: From the nonlinear Talbot effect to the formation of vorticity, *Phys. Rev. A* **63**, 043613 (2001).
- [42] S. P. Cockburn, A. Negretti, N. P. Proukakis, and C. Henkel, Comparison between microscopic methods for finite-temperature Bose gases, *Phys. Rev. A* **83**, 043619 (2011).
- [43] S. P. Cockburn, D. Gallucci, and N. P. Proukakis, Quantitative study of quasi-one-dimensional Bose gas experiments via the stochastic Gross-Pitaevskii equation, *Phys. Rev. A* **84**, 023613 (2011).

- [44] Y. Kagan, E. L. Surkov, and G. V. Shlyapnikov, Evolution of a Bose-condensed gas under variations of the confining potential, *Phys. Rev. A* **54**, R1753 (1996).
- [45] P. A. Ruprecht, M. J. Holland, K. Burnett, and M. Edwards, Time-dependent solution of the nonlinear Schrödinger equation for Bose-condensed trapped neutral atoms, *Phys. Rev. A* **51**, 4704 (1995).
- [46] N. G. Parker, N. P. Proukakis, C. G. Barenghi, and C. S. Adams, Dynamical instability of a dark soliton in a quasi-one-dimensional Bose-Einstein condensate perturbed by an optical lattice, *J. Phys. B: At. Mol. Opt. Phys.* **37**, S175 (2004).
- [47] N. G. Parker, N. P. Proukakis, and C. S. Adams, Dark soliton decay due to trap anharmonicity in atomic Bose-Einstein condensates, *Phys. Rev. A* **81**, 033606 (2010).
- [48] N. G. Parker, N. P. Proukakis, M. Leadbeater, and C. S. Adams, Soliton-Sound Interactions in Quasi-One-Dimensional Bose-Einstein Condensates, *Phys. Rev. Lett.* **90**, 220401 (2003).
- [49] T. Bland, N. G. Parker, N. P. Proukakis, and B. A. Malomed, Probing quasi-integrability of the Gross-Pitaevskii equation in a harmonic-oscillator potential, *J. Phys. B: At. Mol. Opt. Phys.* **51**, 205303 (2018).
- [50] A. D. Martin, C. S. Adams, and S. A. Gardiner, Bright solitary-matter-wave collisions in a harmonic trap: Regimes of solitonlike behavior, *Phys. Rev. A* **77**, 013620 (2008).
- [51] A. Weller, J. P. Ronzheimer, C. Gross, J. Esteve, M. K. Oberthaler, D. J. Frantzeskakis, G. Theocharis, and P. G. Kevrekidis, Experimental Observation of Oscillating and Interacting Matter wave Dark Solitons, *Phys. Rev. Lett.* **101**, 130401 (2008).
- [52] C. Becker, S. Stellmer, P. Soltan-Panahi, S. Dörscher, M. Baumert, E. M. Richter, J. Kronjäger, K. Bongs, and K. Sengstock, Oscillations and interactions of dark and dark-bright solitons in Bose-Einstein condensates, *Nat. Phys.* **4**, 496 (2008).
- [53] T. Busch and J. R. Anglin, Motion of Dark Solitons in Trapped Bose-Einstein Condensates, *Phys. Rev. Lett.* **84**, 2298 (2000).
- [54] G. Huang, J. Szeftel, and S. Zhu, Dynamics of dark solitons in quasi-one-dimensional Bose-Einstein condensates, *Phys. Rev. A* **65**, 053605 (2002).
- [55] D. J. Frantzeskakis, Dark solitons in atomic Bose-Einstein condensates: From theory to experiments, *J. Phys. A: Math. Theor.* **43**, 213001 (2010).
- [56] Y. Castin and R. Dum, Bose-Einstein Condensates in Time Dependent Traps, *Phys. Rev. Lett.* **77**, 5315 (1996).
- [57] Y. Kagan, E. L. Surkov, and G. V. Shlyapnikov, Evolution of a Bose gas in anisotropic time-dependent traps, *Phys. Rev. A* **55**, R18 (1997).
- [58] A. Sinatra, P. O. Fedichev, Y. Castin, J. Dalibard, and G. V. Shlyapnikov, Dynamics of Two Interacting Bose-Einstein Condensates, *Phys. Rev. Lett.* **82**, 251 (1999).
- [59] F. Dalfovo, S. Giorgini, L. P. Pitaevskii, and S. Stringari, Theory of Bose-Einstein condensation in trapped gases, *Rev. Mod. Phys.* **71**, 463 (1999).
- [60] K. Góral, M. Gajda, and K. Rzażewski, Thermodynamics of an interacting trapped Bose-Einstein gas in the classical field approximation, *Phys. Rev. A* **66**, 051602(R) (2002).
- [61] B. Damski and W. H. Zurek, Soliton Creation During A Bose-Einstein Condensation, *Phys. Rev. Lett.* **104**, 160404 (2010).
- [62] P. Grisins and I. E. Mazets, Thermalization in a one-dimensional integrable system, *Phys. Rev. A* **84**, 053635 (2011).
- [63] S. Burger, K. Bongs, S. Dettmer, W. Ertmer, K. Sengstock, A. Sanpera, G. V. Shlyapnikov, and M. Lewenstein, Dark Solitons in Bose-Einstein Condensates, *Phys. Rev. Lett.* **83**, 5198 (1999).
- [64] V. Shukla and S. Nazarenko, Nonequilibrium Bose-Einstein condensation, *Phys. Rev. A* **105**, 033305 (2022).
- [65] A. Paredes, J. R. Salgueiro, and H. Michinel, On vortex and dark solitons in the cubic-quintic nonlinear Schrödinger equation, *Physica D* **437**, 133340 (2022).
- [66] A. Paredes, J. R. Salgueiro, and H. Michinel, Polygons of quantized vortices in Bose-Einstein condensates with a circular trap, *Phys. Rev. E* **107**, 044215 (2023).
- [67] A. Biasi, P. Bizoń, B. Craps, and O. Evnin, Exact lowest-Landau-level solutions for vortex precession in Bose-Einstein condensates, *Phys. Rev. A* **96**, 053615 (2017).
- [68] P. Gérard, P. Germain, and L. Thomann, On the cubic lowest Landau level equation, *Arch. Ration. Mech. Anal.* **231**, 1073 (2019).
- [69] A. Biasi, P. Bizoń, B. Craps, and O. Evnin, Two infinite families of resonant solutions for the Gross-Pitaevskii equation, *Phys. Rev. E* **98**, 032222 (2018).
- [70] A. Biasi, O. Evnin, and B. A. Malomed, Fermi-Pasta-Ulam phenomena and persistent breathers in the harmonic trap, *Phys. Rev. E* **104**, 034210 (2021).
- [71] A. Biasi, P. Bizoń, and O. Evnin, Solvable cubic resonant systems, *Commun. Math. Phys.* **369**, 433 (2019).
- [72] O. Evnin, Breathing modes, quartic nonlinearities and effective resonant systems, *SIGMA* **16**, 034 (2020).
- [73] L. P. Pitaevskii, Dynamics of collapse of a confined Bose gas, *Phys. Lett. A* **221**, 14 (1996).
- [74] L. P. Pitaevskii and A. Rosch, Breathing modes and hidden symmetry of trapped atoms in two dimensions, *Phys. Rev. A* **55**, R853 (1997).
- [75] A. Biasi, P. Bizoń, and O. Evnin, Complex plane representations and stationary states in cubic and quintic resonant systems, *J. Phys. A: Math. Theor.* **52**, 435201 (2019).
- [76] D. S. Petrov, Quantum Mechanical Stabilization of a Collapsing Bose-Bose Mixture, *Phys. Rev. Lett.* **115**, 155302 (2015).
- [77] Z. Luo, W. Pang, B. Liu, Y. Li, and B. A. Malomed, A new form of liquid matter: Quantum droplets, *Front. Phys.* **16**, 32201 (2021).
- [78] S. Nazarenko, *Wave Turbulence* (Springer Science & Business Media, Cham, 2011).
- [79] P. Walczak, S. Randoux, and P. Suret, Optical Rogue Waves in Integrable Turbulence, *Phys. Rev. Lett.* **114**, 143903 (2015).
- [80] S. Randoux, P. Walczak, M. Onorato, and P. Suret, Nonlinear random optical waves: Integrable turbulence, rogue waves and intermittency, *Physica D* **333**, 323 (2016).
- [81] D. S. Agafontsev, S. Randoux, and P. Suret, Extreme rogue wave generation from narrowband partially coherent waves, *Phys. Rev. E* **103**, 032209 (2021).
- [82] V. E. Zakharov, Turbulence in integrable systems, *Stud. Appl. Math.* **122**, 219-234 (2009).
- [83] D. S. Agafontsev and V. E. Zakharov, Integrable turbulence and formation of rogue waves, *Nonlinearity* **28**, 2791 (2015).

- [84] A. A. Gelash and D. S. Agafontsev, Strongly interacting soliton gas and formation of rogue waves, *Phys. Rev. E* **98**, 042210 (2018).
- [85] M. A. Garrido, R. Grande, K. M. Kurianski, and G. Staffilani, Large deviations principle for the cubic NLS equation, [arXiv:2110.15748](https://arxiv.org/abs/2110.15748) [Commun. Pure Appl. Math. (to be published)].
- [86] P. Aschieri, J. Garnier, C. Michel, V. Doya, and A. Picozzi, Condensation and thermalization of classical optical waves in a waveguide, *Phys. Rev. A* **83**, 033838 (2011).
- [87] A. Fusaro, J. Garnier, K. Krupa, G. Millot, and A. Picozzi, Dramatic Acceleration of Wave Condensation Mediated by Disorder in Multimode Fibers, *Phys. Rev. Lett.* **122**, 123902 (2019).
- [88] K. Baudin, A. Fusaro, K. Krupa, J. Garnier, S. Rica, G. Millot, and A. Picozzi, Classical Rayleigh-Jeans Condensation of Light Waves: Observation and Thermodynamic Characterization, *Phys. Rev. Lett.* **125**, 244101 (2020).
- [89] K. Baudin, J. Garnier, A. Fusaro, N. Berti, C. Michel, K. Krupa, G. Millot, and A. Picozzi, Observation of Light thermalization to Negative Temperature Rayleigh-Jeans Equilibrium States in Multimode Optical Fibers, *Phys. Rev. Lett.* **130**, 063801 (2023).
- [90] K. Baudin, J. Garnier, A. Fusaro, C. Michel, K. Krupa, G. Millot, and A. Picozzi, Rayleigh-Jeans thermalization vs beam cleaning in multimode optical fibers, *Opt. Commun.* **545**, 129716 (2023).
- [91] A. Picozzi, J. Garnier, T. Hansson, P. Suret, S. Randoux, G. Millot, and D. N. Christodoulides, Optical wave turbulence: Towards a unified nonequilibrium thermodynamic formulation of statistical nonlinear optics, *Phys. Rep.* **542**, 1-132 (2014).
- [92] G. A. El, Soliton gas in integrable dispersive hydrodynamics, *J. Stat. Mech.: Theory Exp.* (2021) 114001.
- [93] J. A. Murdock, *Perturbations: Theory and Methods* (Wiley, New York, NY, 1991).
- [94] P. Germain, Z. Hani, and L. Thomann, On the continuous resonant equation for NLS. I. Deterministic analysis, *J. Math. Pure Appl.* **105**, 131 (2016).
- [95] P. Bizoń, O. Evnin, and F. Ficek, A nonrelativistic limit for AdS perturbations, *J. High Energy Phys.* **12** (2018) 113.
- [96] F. Kh. Abdullaev and M. Salerno, Gap-Townes solitons and localized excitations in low-dimensional Bose-Einstein condensate in optical lattices, *Phys. Rev. A* **72**, 033617 (2005).
- [97] A. S. Reyna and C. B. de Araújo, High-order optical nonlinearities in plasmonic nanocomposites—A review, *Adv. Opt. Photon.* **9**, 720 (2017).
- [98] A. F. Biasi, J. Mas, and A. Paredes, Delayed collapses of BECs in relation to AdS gravity, *Phys. Rev. E* **95**, 032216 (2017).
- [99] S. Yu. Dubov, V. M. Eleonskii, and N. E. Kulagin, Equidistant spectra of anharmonic oscillators, *Chaos* **4**, 47 (1994).
- [100] M. Ávila-Aoki, C. Cisneros, R. P. Martínez-y-Romero, H. N. Núñez-Yépez, and A. L. Salas-Brito, Classical and quantum motion in an inverse square potential, *Phys. Lett. A* **373**, 418 (2009).
- [101] J. Williams, R. Walser, J. Cooper, E. Cornell, and M. Holland, Nonlinear Josephson-type oscillations of a driven, two-component Bose-Einstein condensate, *Phys. Rev. A* **59**, R31 (1999).
- [102] N. Hacker and B. A. Malomed, Nonlinear dynamics of wave packets in tunnel-coupled harmonic-oscillator traps, *Symmetry* **13**, 372 (2021).
- [103] N. Hacker and B. A. Malomed, Trapping wave fields in an expulsive potential by means of linear coupling, *Phys. Rev. E* **105**, 034213 (2022).
- [104] M. C. P. dos Santos and W. B. Cardoso, Anderson localization induced by interaction in linearly coupled binary Bose-Einstein condensates, *Phys. Rev. E* **103**, 052210 (2021).
- [105] O. Evnin, Resonant Hamiltonian systems and weakly nonlinear dynamics in AdS spacetimes, *Class. Quant. Gravity* **38**, 203001 (2021).
- [106] V. Zakharov, F. Dias, and A. Pushkarev, One-dimensional wave turbulence, *Phys. Rep.* **398**, 1 (2004).
- [107] F. Mangini, M. Gervaziev, M. Ferraro, D. S. Kharenko, M. Zitelli, Y. Sun, V. Couderc, E. V. Podivilov, S. A. Babin, and S. Wabnitz, Statistical mechanics of beam self-cleaning in GRIN multimode optical fibers, *Opt. Express* **30**, 10850 (2022).
- [108] H. Pourbeyram, P. Sidorenko, F. O. Wu, N. Bender, L. Wright, D. N. Christodoulides, and F. Wise, Direct observations of thermalization to a Rayleigh-Jeans distribution in multimode optical fibres, *Nat. Phys.* **18**, 685 (2022).
- [109] J. Amette Estrada, M. E. Brachet, and P. D. Mininni, Turbulence in rotating Bose-Einstein condensates, *Phys. Rev. A* **105**, 063321 (2022).
- [110] J. P. Boyd, *Chebyshev and Fourier Spectral Methods* (Courier Corporation, Chelmsford, MA, 2001).
- [111] A. A. Semenova, S. A. Dyachenko, A. O. Korotkevich, and P. M. Lushnikov, Comparison of split-step and Hamiltonian integration methods for simulation of the nonlinear Schrödinger equation, *J. Comput. Phys.* **427**, 110061 (2021).
- [112] B. Craps, O. Evnin, and J. Vanhoof, Ultraviolet asymptotics and singular dynamics of AdS perturbations, *J. High Energy Phys.* **10** (2015) 079.
- [113] B. Craps, O. Evnin, P. Jai-akson, and J. Vanhoof, Ultraviolet asymptotics for quasiperiodic AdS4 perturbations, *J. High Energy Phys.* **10** (2015) 080.
- [114] O. Evnin and P. Jai-akson, Detailed ultraviolet asymptotics for AdS scalar field perturbations, *J. High Energy Phys.* **04** (2016) 054.
- [115] I. S. Gradshteyn and I. M. Ryzhik, *Table of Integrals, Series, and Products*, 7th ed. (Elsevier, Amsterdam, 2007).
- [116] Y. Pomeau, Asymptotic time behaviour of nonlinear classical field equations, *Nonlinearity* **5**, 707 (1992).
- [117] Y. Pomeau, Long time behavior of solutions of nonlinear classical field equations: The example of NLS defocusing, *Physica D* **61**, 227 (1992).
- [118] R. Jordan and C. Josserand, Self-organization in nonlinear wave turbulence, *Phys. Rev. E* **61**, 1527 (2000).